SUPPORTING MATERIAL

Analysis of RNA Cleavage by MALDI-TOF Mass Spectrometry

Jeff C. Joyner,[1,2] Kevin D. Keuper, [1] and J. A. Cowan[1,2,3]*

Contribution from [1] Evans Laboratory of Chemistry, Ohio State University, 100 West 18th Avenue, Columbus, Ohio 43210; [2] The Ohio State Biochemistry Program, 784 Biological Sciences 484 W. 12th Avenue, Columbus, Ohio 43210; and [3] MetalloPharm LLC, 1790 Riverstone Drive, Delaware, OH 43015

Table of Contents for Supporting Information

Nascent 3' Overhangs								Nascent 5' Overhangs			
3'-OH		2,3-cyclic phosphate		3'-phosphate		3'-phosphoglycolate		5'-OH		5'-phosphate	
m/z (Da)	nucl. pos.	m/z (Da)	nucl. pos.	m/z (Da)	nucl. pos.	m/z (Da)	nucl. pos.	m/z (Da)	nucl. pos.	m/z (Da)	nucl. pos.
12171.52	**36**										
11866.34	35	11928.3	35	11946.32	35	12004.36	35	11327.86	2	11407.84	2
11561.16	34	11623.12	34	11641.14	34	11699.18	34	11021.7	3	11101.68	3
11215.95	33	11277.91	33	11295.93	33	11353.97	33	10676.49	4	10756.47	4
10870.74	32	10932.7	32	10950.72	32	11008.76	32	10331.28	5	10411.26	5
10541.53	31	10603.49	31	10621.51	31	10679.55	31	10025.11	6	10105.09	6
10236.35	30	10298.31	30	10316.33	30	10374.37	30	9719.93	7	9799.91	7
9907.14	29	9969.1	29	9987.12	29	10045.16	29	9413.76	8	9493.74	8
9600.97	28	9662.93	28	9680.95	28	9738.99	28	9068.55	9	9148.53	9
9255.76	27	9317.72	27	9335.74	27	9393.78	27	8723.34	10	8803.32	10
8910.55	26	8972.51	26	8990.53	26	9048.57	26	8378.13	11	8458.11	11
8605.37	25	8667.33	25	8685.35	25	8743.39	25	8072.95	12	8152.93	12
8276.16	24	8338.12	24	8356.14	24	8414.18	24	7727.74	13	7807.72	13
7930.95	23	7992.91	23	8010.93	23	8068.97	23	7422.56	14	7502.54	14
7624.78	22	7686.74	22	7704.76	22	7762.8	22	7093.35	15	7173.33	15
7319.6	21	7381.56	21	7399.58	21	7457.62	21	6748.14	16	6828.12	16
6974.39	20	7036.35	20	7054.37	20	7112.41	20	6442.96	17	6522.94	17
6645.18	19	6707.14	19	6725.16	19	6783.2	19	6097.75	18	6177.73	18
6315.97	18	6377.93	18	6395.95	18	6453.99	18	**5792.57**	**19**	5872.55	19
6010.79	17	6072.75	17	6090.77	17	6148.81	17	5463.36	20	5543.34	20
5665.58	16	5727.54	16	5745.56	16	5803.6	16	5134.15	21	5214.13	21
5360.39	15	5422.35	15	5440.37	15	5498.41	15	4788.94	22	4868.92	22
5015.18	14	5077.14	14	5095.16	14	5153.2	14	4483.76	23	4563.74	23
4685.97	13	**4747.93**	**13**	4765.95	13	4823.99	13	4177.59	24	4257.57	24
4380.79	12	4442.75	12	4460.77	12	4518.81	12	3832.38	25	3912.36	25
4035.58	11	4097.54	11	4115.56	11	4173.6	11	3503.17	26	3583.15	26
3730.4	10	3792.36	10	3810.38	10	3868.42	10	3197.99	27	3277.97	27
3385.19	9	3447.15	9	3465.17	9	3523.21	9	2852.78	28	2932.76	28
3039.98	8	**3101.94**	**8**	3119.96	8	3178	8	2507.57	29	2587.55	29
2694.77	7	**2756.73**	**7**	2774.75	7	2832.79	7	**2201.4**	**30**	2281.38	30
2388.6	6	**2450.56**	**6**	2468.58	6	2526.62	6	1872.19	31	1952.17	31
2083.42	5	**2145.38**	**5**	2163.4	5	2221.44	5	**1567.01**	**32**	1646.99	32
1777.25	4	1839.21	4	1857.23	4	1915.27	4	1237.8	33	1317.78	33
1432.04	3	**1494**	**3**	1512.02	3	1570.06	3	892.59	34	972.57	34
1086.83	2	1148.79	2	1166.81	2	1224.85	2	547.38	35	627.36	35
780.66	1	842.62	1	860.64	1	918.68	1	242.2	36	322.18	36

Table SM1. Predicted masses for products ions (z = -1) resulting from cleavage of Fl-RRE RNA (36-mer). The predicted masses shown here correspond to $[RNA]^{1-}$ fragments terminated with one of the listed nascent overhangs, at one of the positions shown. These masses were used for assignment of peaks in mass spectra. All fragments with nascent 3' overhangs were terminated at the 5' end with fluorescein; all fragments with nascent 5' overhangs were terminated at the 3' end with a 3'-hydroxyl group. The Fl-RRE RNA is similarly terminated at the 5' end with fluorescein and at the 3' end with a 3'-hydroxyl group (unreacted; m/z = 12171.53 Da). Peaks used for internal calibration are shown in bold (also included $[Fl\text{-}RRE - 2H]^{2-}$ with m/z = 6085.26 Da).

Nascent 3' Overhangs								Nascent 5' Overhangs			
3'-OH		2,3-cyclic phosphate		3'-phosphate		3'-phosphoglycolate		5'-OH		5'-phosphate	
m/z (Da)	nucl. pos.	m/z (Da)	nucl. pos.	m/z (Da)	nucl. pos.	m/z (Da)	nucl. pos.	m/z (Da)	nucl. pos.	m/z (Da)	nucl. pos.
9175.71	**27**										
8870.53	26	8932.49	26	8950.51	26	9008.55	26	8293.02	2	8373	2
8565.35	25	8627.31	25	8645.33	25	8703.37	25	7947.81	3	8027.79	3
8220.14	24	8282.1	24	8300.12	24	8358.16	24	7642.63	4	7722.61	4
7914.96	23	7976.92	23	7994.94	23	8052.98	23	7297.42	5	7377.4	5
7608.79	22	7670.75	22	7688.77	22	7746.81	22	6991.25	6	7071.23	6
7263.58	21	7325.54	21	7343.56	21	7401.6	21	6686.07	7	6766.05	7
6934.37	20	6996.33	20	7014.35	20	7072.39	20	6356.86	8	6436.84	8
6605.16	19	6667.12	19	6685.14	19	6743.18	19	6051.68	9	6131.66	9
6259.95	18	6321.91	18	6339.93	18	6397.97	18	5722.47	10	5802.45	10
5953.78	17	6015.74	17	6033.76	17	6091.8	17	5417.29	11	5497.27	11
5608.57	16	5670.53	16	5688.55	16	5746.59	16	5112.11	12	5192.09	12
5263.36	15	5325.32	15	5343.34	15	5401.38	15	4805.94	13	4885.92	13
4918.15	14	4980.11	14	4998.13	14	5056.17	14	4499.77	14	4579.75	14
4612.97	13	4674.93	13	4692.95	13	4750.99	13	4194.58	15	4274.56	15
4306.8	12	4368.76	12	4386.78	12	4444.82	12	3849.37	16	3929.35	16
4000.63	11	4062.59	11	4080.61	11	4138.65	11	3504.16	17	3584.14	17
3695.45	10	3757.41	10	3775.43	10	3833.47	10	**3158.95**	**18**	3238.93	18
3390.26	9	3452.22	9	3470.24	9	3528.28	9	2852.78	19	2932.76	19
3061.05	8	**3123.01**	**8**	3141.03	8	3199.07	8	2507.57	20	2587.55	20
2755.87	7	2817.83	7	2835.85	7	2893.89	7	2178.36	21	2258.34	21
2426.66	6	**2488.62**	**6**	2506.64	6	2564.68	6	1849.15	22	1929.13	22
2121.48	5	2183.44	5	2201.46	5	2259.5	5	1503.94	23	1583.92	23
1815.31	4	**1877.27**	**4**	1895.29	4	1953.33	4	1197.77	24	1277.75	24
1470.1	3	1532.06	3	1550.08	3	1608.12	3	892.59	25	972.57	25
1164.92	2	**1226.88**	**2**	1244.9	2	1302.94	2	547.38	26	627.36	26
819.71	1	881.67	1	899.69	1	957.73	1	242.2	27	322.18	27

Table SM2. Predicted masses for products ions (z = -1) resulting from cleavage of Fl-16S RNA (27-mer). The predicted masses shown here correspond to $[RNA]^{1-}$ fragments terminated with one of the listed nascent overhangs, at one of the positions shown. These masses were used for assignment of peaks in mass spectra. All fragments with nascent 3' overhangs were terminated at the 5' end with fluorescein; all fragments with nascent 5' overhangs were terminated at the 3' end with a 3'-hydroxyl group. The Fl-16S RNA is similarly terminated at the 5' end with fluorescein and at the 3' end with a 3'-hydroxyl group (unreacted; m/z = 9175.71 Da). Peaks used for internal calibration are shown in bold (also included $[Fl\text{-}16S - 2H]^{2-}$ with m/z = 4587.35 Da).

Nascent 3' Overhangs								Nascent 5' Overhangs			
3'-OH		2,3-cyclic phosphate		3'-phosphate		3'-phosphoglycolate		5'-OH		5'-phosphate	
m/z (Da)	nucl. pos.	m/z (Da)	nucl. pos.	m/z (Da)	nucl. pos.	m/z (Da)	nucl. pos.	m/z (Da)	nucl. pos.	m/z (Da)	nucl. pos.
282.22	1	344.18	1	362.2	1	420.24	1	11021.7	1		
627.43	2	689.39	2	707.41	2	765.45	2	10676.49	2	10756.47	2
933.6	3	995.56	3	1013.58	3	1071.62	3	10331.28	3	10411.26	3
1238.78	4	1300.74	4	1318.76	4	1376.8	4	10025.11	4	10105.09	4
1544.95	5	1606.91	5	1624.93	5	1682.97	5	9719.93	5	9799.91	5
1890.16	6	1952.12	6	1970.14	6	2028.18	6	9413.76	6	9493.74	6
2235.37	7	2297.33	7	2315.35	7	2373.39	7	9068.55	7	9148.53	7
2580.58	8	2642.54	8	2660.56	8	2718.6	8	8723.34	8	8803.32	8
2885.76	9	2947.72	9	2965.74	9	3023.78	9	8378.13	9	8458.11	9
3230.97	10	3292.93	10	3310.95	10	3368.99	10	8072.95	10	8152.93	10
3536.15	11	3598.11	11	3616.13	11	3674.17	11	7727.74	11	7807.72	11
3865.36	12	3927.32	12	3945.34	12	4003.38	12	7422.56	12	7502.54	12
4210.57	13	4272.53	13	4290.55	13	4348.59	13	7093.35	13	7173.33	13
4515.76	14	4577.72	14	4595.74	14	4653.78	14	6748.14	14	6828.12	14
4860.97	15	4922.93	15	4940.95	15	4998.99	15	6442.96	15	6522.94	15
5166.15	16	5228.11	16	5246.13	16	5304.17	16	6097.75	16	6177.73	16
5495.36	17	5557.32	17	5575.34	17	5633.38	17	5792.57	17	5872.55	17
5824.57	18	5886.53	18	5904.55	18	5962.59	18	5463.36	18	5543.34	18
6169.78	19	6231.74	19	6249.76	19	6307.8	19	5134.15	19	5214.13	19
6474.96	20	6536.92	20	6554.94	20	6612.98	20	4788.94	20	4868.92	20
6781.13	21	6843.09	21	6861.11	21	6919.15	21	4483.76	21	4563.74	21
7126.34	22	7188.3	22	7206.32	22	7264.36	22	4177.59	22	4257.57	22
7455.55	23	7517.51	23	7535.53	23	7593.57	23	3832.38	23	3912.36	23
7760.73	24	7822.69	24	7840.71	24	7898.75	24	3503.17	24	3583.15	24
8105.94	25	8167.9	25	8185.92	25	8243.96	25	3197.99	25	3277.97	25
8451.15	26	8513.11	26	8531.13	26	8589.17	26	2852.78	26	2932.76	26
8757.32	27	8819.28	27	8837.3	27	8895.34	27	2507.57	27	2587.55	27
9086.53	28	9148.49	28	9166.51	28	9224.55	28	2201.4	28	2281.38	28
9391.71	29	9453.67	29	9471.69	29	9529.73	29	1872.19	29	1952.17	29
9720.92	30	9782.88	30	9800.9	30	9858.94	30	1567.01	30	1646.99	30
10066.13	31	10128.09	31	10146.11	31	10204.15	31	1237.8	31	1317.78	31
10411.34	32	10473.3	32	10491.32	32	10549.36	32	892.59	32	972.57	32
10716.52	33	10778.48	33	10796.5	33	10854.54	33	547.38	33	627.36	33
11021.7	34							242.2	34	322.18	34

Table SM3. Predicted masses for products ions (z = -1) resulting from cleavage of unlabeled RRE RNA (34-mer). The predicted masses shown here correspond to $[RNA]^{1-}$ fragments terminated with one of the listed nascent overhangs, at one of the positions shown. These masses were used for assignment of peaks in mass spectra. All fragments with nascent 3' overhangs were terminated at the 5' end with a 5'-hydroxyl group; all fragments with nascent 5' overhangs were terminated at the 3' end with a 3'-hydroxyl group. The full length RRE RNA is similarly terminated at both ends with hydroxyl groups.

Mass-Matching Information			Product Assignment and Abundance			
Theoretical Mass (Da)	**Observed Mass (Da)**	**Mass Error (ppm)**	**Nucleotide Position**	**Overhang Type**	**Peak Area**	**Peak Area Fraction**
780.66	no match	no match	1	3'-OH	0	0
1086.83	no match	no match	2	3'-OH	0	0
1432.04	no match	no match	3	3'-OH	0	0
1777.25	no match	no match	4	3'-OH	0	0
2083.42	no match	no match	5	3'-OH	0	0
2388.6	no match	no match	6	3'-OH	0	0
2694.77	no match	no match	7	3'-OH	0	0
3039.98	no match	no match	8	3'-OH	0	0
3385.19	no match	no match	9	3'-OH	0	0
3730.4	no match	no match	10	3'-OH	0	0
4035.58	no match	no match	11	3'-OH	0	0
4380.79	no match	no match	12	3'-OH	0	0
4685.97	no match	no match	13	3'-OH	0	0
5015.18	no match	no match	14	3'-OH	0	0
5360.39	no match	no match	15	3'-OH	0	0
5665.58	no match	no match	16	3'-OH	0	0
6010.79	no match	no match	17	3'-OH	0	0
6315.97	no match	no match	18	3'-OH	0	0
6645.18	no match	no match	19	3'-OH	0	0
6974.39	no match	no match	20	3'-OH	0	0
7319.6	no match	no match	21	3'-OH	0	0
7624.78	no match	no match	22	3'-OH	0	0
7930.95	no match	no match	23	3'-OH	0	0
8276.16	no match	no match	24	3'-OH	0	0
8605.37	no match	no match	25	3'-OH	0	0
8910.55	no match	no match	26	3'-OH	0	0
9255.76	no match	no match	27	3'-OH	0	0
9600.97	no match	no match	28	3'-OH	0	0
9907.14	no match	no match	29	3'-OH	0	0
10236.35	no match	no match	30	3'-OH	0	0
10541.53	no match	no match	31	3'-OH	0	0
10870.74	no match	no match	32	3'-OH	0	0
11215.95	no match	no match	33	3'-OH	0	0
11561.16	no match	no match	34	3'-OH	0	0
11866.34	no match	no match	35	3'-OH	0	0
12171.52	12171.55818	3.1	36	3'-OH	1948.371456	0.008537898

842.62	no match	no match	1	2,3-cyclic phosphate	0	0
1148.79	1148.676728	-98.6	2	2,3-cyclic phosphate	19.9849813	8.75756E-05
1494	1494.177343	118.7	3	2,3-cyclic phosphate	86.96068556	0.000381068
1839.21	1839.13182	-42.5	4	2,3-cyclic phosphate	71.38448349	0.000312812
2145.38	2145.700106	149.2	5	2,3-cyclic phosphate	161.9090032	0.000709496
2450.56	2450.833115	111.5	6	2,3-cyclic phosphate	1222.599179	0.005357514
2756.73	no match	no match	7	2,3-cyclic phosphate	0	0
3101.94	3102.406808	150.5	8	2,3-cyclic phosphate	2015.349322	0.008831399
3447.15	3447.535372	111.8	9	2,3-cyclic phosphate	546.5299809	0.002394932
3792.36	3792.399381	10.4	10	2,3-cyclic phosphate	107.4578944	0.000470888
4097.54	4097.845766	74.6	11	2,3-cyclic phosphate	119.5056344	0.000523682
4442.75	no match	no match	12	2,3-cyclic phosphate	0	0
4747.93	4748.310105	80.1	13	2,3-cyclic phosphate	459.2131279	0.002012303
5077.14	no match	no match	14	2,3-cyclic phosphate	0	0
5422.35	no match	no match	15	2,3-cyclic phosphate	0	0
5727.54	no match	no match	16	2,3-cyclic phosphate	0	0
6072.75	no match	no match	17	2,3-cyclic phosphate	0	0
6377.93	no match	no match	18	2,3-cyclic phosphate	0	0
6707.14	no match	no match	19	2,3-cyclic phosphate	0	0
7036.35	no match	no match	20	2,3-cyclic phosphate	0	0
7381.56	no match	no match	21	2,3-cyclic phosphate	0	0
7686.74	no match	no match	22	2,3-cyclic phosphate	0	0
7992.91	no match	no match	23	2,3-cyclic phosphate	0	0
8338.12	no match	no match	24	2,3-cyclic phosphate	0	0
8667.33	no match	no match	25	2,3-cyclic phosphate	0	0
8972.51	no match	no match	26	2,3-cyclic phosphate	0	0
9317.72	no match	no match	27	2,3-cyclic phosphate	0	0
9662.93	no match	no match	28	2,3-cyclic phosphate	0	0
9969.1	no match	no match	29	2,3-cyclic phosphate	0	0
10298.31	no match	no match	30	2,3-cyclic phosphate	0	0
10603.49	no match	no match	31	2,3-cyclic phosphate	0	0
10932.7	no match	no match	32	2,3-cyclic phosphate	0	0
11277.91	no match	no match	33	2,3-cyclic phosphate	0	0
11623.12	no match	no match	34	2,3-cyclic phosphate	0	0
11928.3	no match	no match	35	2,3-cyclic phosphate	0	0
NA	no match	no match	36	2,3-cyclic phosphate	0	0
860.64	no match	no match	1	3'-phosphate	0	0
1166.81	no match	no match	2	3'-phosphate	0	0
1512.02	no match	no match	3	3'-phosphate	0	0
1857.23	1857.221253	-4.7	4	3'-phosphate	691.5150369	0.003030266
2163.4	2163.515727	53.5	5	3'-phosphate	9132.265028	0.040018213

2468.58	2468.739643	64.7	6	3'-phosphate	15694.70981	0.068775297
2774.75	2774.987205	85.5	7	3'-phosphate	22471.69868	0.098472528
3119.96	3120.203586	78.1	8	3'-phosphate	15805.23257	0.069259615
3465.17	3465.353903	53.1	9	3'-phosphate	3946.3796	0.017293307
3810.38	3810.794395	108.8	10	3'-phosphate	429.0367276	0.001880068
4115.56	4116.120122	136.1	11	3'-phosphate	237.7550917	0.001041859
4460.77	4460.625181	-32.5	12	3'-phosphate	126.0200837	0.000552229
4765.95	4766.488901	113.1	13	3'-phosphate	208.2846982	0.000912718
5095.16	5095.167286	1.4	14	3'-phosphate	70.74809863	0.000310023
5440.37	5440.752039	70.2	15	3'-phosphate	70.71147749	0.000309863
5745.56	5746.194232	110.4	16	3'-phosphate	79.74872857	0.000349464
6090.77	no match	no match	17	3'-phosphate	0	0
6395.95	no match	no match	18	3'-phosphate	0	0
6725.16	no match	no match	19	3'-phosphate	0	0
7054.37	no match	no match	20	3'-phosphate	0	0
7399.58	no match	no match	21	3'-phosphate	0	0
7704.76	no match	no match	22	3'-phosphate	0	0
8010.93	no match	no match	23	3'-phosphate	0	0
8356.14	no match	no match	24	3'-phosphate	0	0
8685.35	no match	no match	25	3'-phosphate	0	0
8990.53	no match	no match	26	3'-phosphate	0	0
9335.74	no match	no match	27	3'-phosphate	0	0
9680.95	no match	no match	28	3'-phosphate	0	0
9987.12	no match	no match	29	3'-phosphate	0	0
10316.33	no match	no match	30	3'-phosphate	0	0
10621.51	no match	no match	31	3'-phosphate	0	0
10950.72	no match	no match	32	3'-phosphate	0	0
11295.93	no match	no match	33	3'-phosphate	0	0
11641.14	no match	no match	34	3'-phosphate	0	0
11946.32	no match	no match	35	3'-phosphate	0	0
NA	no match	no match	36	3'-phosphate	0	0
918.68	no match	no match	1	3'-phosphoglycolate	0	0
1224.85	no match	no match	2	3'-phosphoglycolate	0	0
1570.06	no match	no match	3	3'-phosphoglycolate	0	0
1915.27	1915.324956	28.7	4	3'-phosphoglycolate	1536.114549	0.00673136
2221.44	2221.603802	73.7	5	3'-phosphoglycolate	17404.45802	0.076267531
2526.62	2526.845626	89.3	6	3'-phosphoglycolate	37150.11861	0.162794373
2832.79	2833.014314	79.2	7	3'-phosphoglycolate	24951.63066	0.10933976
3178	3178.23388	73.6	8	3'-phosphoglycolate	16011.80409	0.070164826
3523.21	3523.452255	68.8	9	3'-phosphoglycolate	3075.000656	0.013474864
3868.42	3868.78875	95.3	10	3'-phosphoglycolate	849.2317142	0.003721392

4173.6	no match	no match	11	3'-phosphoglycolate	0	0
4518.81	4519.042088	51.4	12	3'-phosphoglycolate	192.569598	0.000843853
4823.99	4823.818951	-35.5	13	3'-phosphoglycolate	123.0122804	0.000539048
5153.2	no match	no match	14	3'-phosphoglycolate	0	0
5498.41	5498.711065	54.8	15	3'-phosphoglycolate	103.2110446	0.000452278
5803.6	no match	no match	16	3'-phosphoglycolate	0	0
6148.81	no match	no match	17	3'-phosphoglycolate	0	0
6453.99	no match	no match	18	3'-phosphoglycolate	0	0
6783.2	no match	no match	19	3'-phosphoglycolate	0	0
7112.41	7112.169407	-33.8	20	3'-phosphoglycolate	88.79963368	0.000389126
7457.62	no match	no match	21	3'-phosphoglycolate	0	0
7762.8	no match	no match	22	3'-phosphoglycolate	0	0
8068.97	no match	no match	23	3'-phosphoglycolate	0	0
8414.18	no match	no match	24	3'-phosphoglycolate	0	0
8743.39	no match	no match	25	3'-phosphoglycolate	0	0
9048.57	no match	no match	26	3'-phosphoglycolate	0	0
9393.78	no match	no match	27	3'-phosphoglycolate	0	0
9738.99	no match	no match	28	3'-phosphoglycolate	0	0
10045.16	no match	no match	29	3'-phosphoglycolate	0	0
10374.37	no match	no match	30	3'-phosphoglycolate	0	0
10679.55	no match	no match	31	3'-phosphoglycolate	0	0
11008.76	no match	no match	32	3'-phosphoglycolate	0	0
11353.97	no match	no match	33	3'-phosphoglycolate	0	0
11699.18	no match	no match	34	3'-phosphoglycolate	0	0
12004.36	no match	no match	35	3'-phosphoglycolate	0	0
NA	no match	no match	36	3'-phosphoglycolate	0	0
NA	no match	no match	1	5'-OH	0	0
11327.86	no match	no match	2	5'-OH	0	0
11021.7	no match	no match	3	5'-OH	0	0
10676.49	no match	no match	4	5'-OH	0	0
10331.28	no match	no match	5	5'-OH	0	0
10025.11	no match	no match	6	5'-OH	0	0
9719.93	no match	no match	7	5'-OH	0	0
9413.76	no match	no match	8	5'-OH	0	0
9068.55	no match	no match	9	5'-OH	0	0
8723.34	no match	no match	10	5'-OH	0	0
8378.13	no match	no match	11	5'-OH	0	0
8072.95	no match	no match	12	5'-OH	0	0
7727.74	no match	no match	13	5'-OH	0	0
7422.56	7421.974566	-78.9	14	5'-OH	78.30586776	0.000343142
7093.35	no match	no match	15	5'-OH	0	0

6748.14	no match	no match	16	5'-OH	0	0
6442.96	no match	no match	17	5'-OH	0	0
6097.75	no match	no match	18	5'-OH	0	0
5792.57	5792.207389	-62.6	19	5'-OH	567.2532745	0.002485743
5463.36	5462.385422	-178.4	20	5'-OH	133.4589669	0.000584826
5134.15	5133.380899	-149.8	21	5'-OH	148.517815	0.000650815
4788.94	4788.004116	-195.4	22	5'-OH	381.1841812	0.001670375
4483.76	4483.037567	-161.1	23	5'-OH	483.8956656	0.002120464
4177.59	no match	no match	24	5'-OH	0	0
3832.38	3831.838834	-141.2	25	5'-OH	1100.619085	0.004822988
3503.17	3502.734975	-124.2	26	5'-OH	914.7354935	0.004008434
3197.99	3197.677233	-97.8	27	5'-OH	6642.141128	0.029106319
2852.78	2852.715205	-22.7	28	5'-OH	3244.762079	0.01421877
2507.57	no match	no match	29	5'-OH	0	0
2201.4	2201.024257	-170.7	30	5'-OH	1964.902418	0.008610337
1872.19	no match	no match	31	5'-OH	0	0
1567.01	no match	no match	32	5'-OH	0	0
1237.8	no match	no match	33	5'-OH	0	0
892.59	no match	no match	34	5'-OH	0	0
547.38	no match	no match	35	5'-OH	0	0
242.2	no match	no match	36	5'-OH	0	0
NA	no match	no match	1	5'-phosphate	0	0
11407.84	no match	no match	2	5'-phosphate	0	0
11101.68	no match	no match	3	5'-phosphate	0	0
10756.47	no match	no match	4	5'-phosphate	0	0
10411.26	no match	no match	5	5'-phosphate	0	0
10105.09	no match	no match	6	5'-phosphate	0	0
9799.91	no match	no match	7	5'-phosphate	0	0
9493.74	no match	no match	8	5'-phosphate	0	0
9148.53	no match	no match	9	5'-phosphate	0	0
8803.32	no match	no match	10	5'-phosphate	0	0
8458.11	no match	no match	11	5'-phosphate	0	0
8152.93	no match	no match	12	5'-phosphate	0	0
7807.72	no match	no match	13	5'-phosphate	0	0
7502.54	no match	no match	14	5'-phosphate	0	0
7173.33	no match	no match	15	5'-phosphate	0	0
6828.12	no match	no match	16	5'-phosphate	0	0
6522.94	6523.053447	17.4	17	5'-phosphate	89.52517336	0.000392305
6177.73	6177.340573	-63.0	18	5'-phosphate	112.999793	0.000495173
5872.55	no match	no match	19	5'-phosphate	0	0
5543.34	5542.905083	-78.5	20	5'-phosphate	157.6384834	0.000690783

5214.13	5213.717271	-79.2	21	5'-phosphate	808.7536572	0.003544014
4868.92	4868.550131	-76.0	22	5'-phosphate	6036.56855	0.026452658
4563.74	4563.388356	-77.1	23	5'-phosphate	8501.901754	0.037255918
4257.57	4257.220846	-82.0	24	5'-phosphate	3625.111927	0.01588549
3912.36	3912.08979	-69.1	25	5'-phosphate	5413.856879	0.023723893
3583.15	3582.747586	-112.3	26	5'-phosphate	2047.538426	0.008972454
3277.97	3277.532532	-133.5	27	5'-phosphate	1484.279898	0.006504217
2932.76	2932.38258	-128.7	28	5'-phosphate	3837.8812	0.016817859
2587.55	2587.712148	62.7	29	5'-phosphate	3021.656977	0.013241109
2281.38	no match	no match	30	5'-phosphate	0	0
1952.17	1952.263488	47.9	31	5'-phosphate	152.0288931	0.000666201
1646.99	1647.140761	91.5	32	5'-phosphate	43.8794809	0.000192283
1317.78	no match	no match	33	5'-phosphate	0	0
972.57	no match	no match	34	5'-phosphate	0	0
627.36	no match	no match	35	5'-phosphate	0	0
322.18	no match	no match	36	5'-phosphate	0	0
unknown	1000.192991	unknown	unknown	unknown	90.71652509	
unknown	1024.669562	unknown	unknown	unknown	-29.6925884	
unknown	1039.43436	unknown	unknown	unknown	24.14009998	
unknown	1053.934414	unknown	unknown	unknown	34.13122436	
unknown	1069.882167	unknown	unknown	unknown	489.3513209	
unknown	1086.250217	unknown	unknown	unknown	3813.317469	
unknown	1101.659453	unknown	unknown	unknown	120.7820136	
unknown	1108.904736	unknown	unknown	unknown	93.921094	
unknown	1124.00714	unknown	unknown	unknown	71.55375436	
unknown	1133.790497	unknown	unknown	unknown	26.65421214	
unknown	1136.358489	unknown	unknown	unknown	23.63199722	
unknown	1165.854354	unknown	unknown	unknown	-6.29728988	
unknown	1179.838319	unknown	unknown	unknown	79.04650475	
unknown	1233.510332	unknown	unknown	unknown	37.27961491	
unknown	1247.174724	unknown	unknown	unknown	196.6719913	
unknown	1263.14571	unknown	unknown	unknown	583.931974	
unknown	1317.359707	unknown	unknown	unknown	21.640908	
unknown	1355.560024	unknown	unknown	unknown	20.71653472	
unknown	1370.493209	unknown	unknown	unknown	32.27658793	
unknown	1386.483356	unknown	unknown	unknown	164.6063434	
unknown	1402.587372	unknown	unknown	unknown	1547.447956	
unknown	1416.490318	unknown	unknown	unknown	70.02387475	
unknown	1424.723702	unknown	unknown	unknown	35.78683123	
unknown	1440.612758	unknown	unknown	unknown	30.77960854	
unknown	1511.685729	unknown	unknown	unknown	29.50911445	

unknown	1566.610509	unknown	unknown	unknown	465.2994219	
unknown	1579.493361	unknown	unknown	unknown	180.759015	
unknown	1606.340372	unknown	unknown	unknown	36.17600065	
unknown	1623.034516	unknown	unknown	unknown	20.46627907	
unknown	1718.726167	unknown	unknown	unknown	348.709257	
unknown	1758.887165	unknown	unknown	unknown	43.82186144	
unknown	1871.590065	unknown	unknown	unknown	9.446150706	
unknown	1929.932864	unknown	unknown	unknown	28.28051184	
unknown	1968.584025	unknown	unknown	unknown	31.23915989	
unknown	1971.961522	unknown	unknown	unknown	63.54064087	
unknown	1982.187724	unknown	unknown	unknown	40.7167382	
unknown	1987.429082	unknown	unknown	unknown	44.74467949	
unknown	1991.243496	unknown	unknown	unknown	37.79707248	
unknown	1996.593954	unknown	unknown	unknown	45.41801614	
unknown	2001.890852	unknown	unknown	unknown	39.31007596	
unknown	2009.386902	unknown	unknown	unknown	76.91657201	
unknown	2014.916877	unknown	unknown	unknown	30.43567252	
unknown	2023.275601	unknown	unknown	unknown	51.07662072	
unknown	2029.681143	unknown	unknown	unknown	125.7186618	
unknown	2178.179229	unknown	unknown	unknown	-327.68893	
unknown	2236.672981	unknown	unknown	unknown	137.0835501	
unknown	2243.180393	unknown	unknown	unknown	316.1129164	
unknown	2258.80587	unknown	unknown	unknown	29.97590942	
unknown	2280.676299	unknown	unknown	unknown	440.2159526	
unknown	2298.186916	unknown	unknown	unknown	162.9054286	
unknown	2304.742186	unknown	unknown	unknown	68.60534076	
unknown	2317.095466	unknown	unknown	unknown	377.2914437	
unknown	2338.354426	unknown	unknown	unknown	538.4354975	
unknown	2350.856313	unknown	unknown	unknown	388.5381762	
unknown	2370.760453	unknown	unknown	unknown	87.17885192	
unknown	2541.373176	unknown	unknown	unknown	-1310.58496	
unknown	2548.483483	unknown	unknown	unknown	-1208.94526	
unknown	2563.630388	unknown	unknown	unknown	-881.789527	
unknown	2577.408212	unknown	unknown	unknown	8608.637868	
unknown	2607.955333	unknown	unknown	unknown	6106.949511	
unknown	2617.309656	unknown	unknown	unknown	43048.49137	
unknown	2629.127298	unknown	unknown	unknown	15558.24052	
unknown	2644.314014	unknown	unknown	unknown	8976.873126	
unknown	2688.374481	unknown	unknown	unknown	360.3229347	
unknown	2699.338356	unknown	unknown	unknown	20.59771314	
unknown	2707.67266	unknown	unknown	unknown	22.09327158	

unknown	2757.444581	unknown	unknown	unknown	1431.897555	
unknown	2789.557577	unknown	unknown	unknown	1268.96941	
unknown	2799.509302	unknown	unknown	unknown	3613.605499	
unknown	2811.455219	unknown	unknown	unknown	-1279.63467	
unknown	2870.23302	unknown	unknown	unknown	-1740.20751	
unknown	2890.813359	unknown	unknown	unknown	1899.615445	
unknown	2904.812734	unknown	unknown	unknown	-31.5745912	
unknown	2912.761248	unknown	unknown	unknown	-597.395143	
unknown	3022.372448	unknown	unknown	unknown	-232.589255	
unknown	3041.993977	unknown	unknown	unknown	200.3018082	
unknown	3054.290182	unknown	unknown	unknown	400.4101123	
unknown	3065.954174	unknown	unknown	unknown	468.9866774	
unknown	3078.020315	unknown	unknown	unknown	944.2477428	
unknown	3135.107258	unknown	unknown	unknown	1523.958415	
unknown	3158.122425	unknown	unknown	unknown	-143.32206	
unknown	3214.252631	unknown	unknown	unknown	984.7318833	
unknown	3293.678138	unknown	unknown	unknown	-327.102533	
unknown	3369.147336	unknown	unknown	unknown	213.6951354	
unknown	3377.517692	unknown	unknown	unknown	86.68170643	
unknown	3384.131534	unknown	unknown	unknown	158.4937202	
unknown	3400.049679	unknown	unknown	unknown	173.8475433	
unknown	3480.656129	unknown	unknown	unknown	176.264323	
unknown	3538.484178	unknown	unknown	unknown	-2.28260888	
unknown	3560.688097	unknown	unknown	unknown	-223.531924	
unknown	3602.977367	unknown	unknown	unknown	397.6536785	
unknown	3619.448723	unknown	unknown	unknown	-11.6441085	
unknown	3686.06181	unknown	unknown	unknown	23.57329675	
unknown	3713.649309	unknown	unknown	unknown	78.93446147	
unknown	3745.962802	unknown	unknown	unknown	45.04616355	
unknown	3846.299735	unknown	unknown	unknown	96.52177333	
unknown	3883.556857	unknown	unknown	unknown	123.4229807	
unknown	3930.050686	unknown	unknown	unknown	351.2166462	
unknown	3948.966547	unknown	unknown	unknown	110.5668399	
unknown	4176.241589	unknown	unknown	unknown	1288.091898	
unknown	4191.091806	unknown	unknown	unknown	267.6094676	
unknown	4213.968859	unknown	unknown	unknown	51.23232897	
unknown	4273.902148	unknown	unknown	unknown	485.8861199	
unknown	4294.44941	unknown	unknown	unknown	97.38480426	
unknown	4441.684106	unknown	unknown	unknown	172.5652913	
unknown	4497.413701	unknown	unknown	unknown	374.9069586	
unknown	4580.925364	unknown	unknown	unknown	554.0391234	

unknown	4600.400185	unknown	unknown	unknown	224.535698	
unknown	4618.571637	unknown	unknown	unknown	54.43201194	
unknown	4802.663955	unknown	unknown	unknown	483.4152525	
unknown	4887.738593	unknown	unknown	unknown	345.3399293	
unknown	4906.752139	unknown	unknown	unknown	140.4235055	
unknown	4940.917293	unknown	unknown	unknown	166.8740241	
unknown	5152.153598	unknown	unknown	unknown	255.6915291	
unknown	5169.05932	unknown	unknown	unknown	77.27809114	
unknown	5231.27596	unknown	unknown	unknown	305.7992614	
unknown	5248.342185	unknown	unknown	unknown	70.80900843	
unknown	5559.046816	unknown	unknown	unknown	102.5444777	
unknown	5805.801307	unknown	unknown	unknown	280.4613142	
unknown	6095.10959	unknown	unknown	unknown	250.5558863	
unknown	6110.636695	unknown	unknown	unknown	108.4119919	
unknown	12187.52966	unknown	unknown	unknown	1194.220106	
unknown	12204.99702	unknown	unknown	unknown	722.1666675	
unknown	12222.24389	unknown	unknown	unknown	316.2455707	

Table SM4. Example output from MassDaddy for one reaction (with subsequent calculation of peak area fractions), showing matching of observed MS peaks with predicted peaks for Fl-RRE RNA cleavage products, which contained the listed nascent overhangs at the listed nucleotide positions (36 nucleotides in the Fl-RRE sequence). Peak assignment was performed by comparison of observed m/z with theoretical m/z, with a mass matching tolerance of 200 ppm (mass matching errors are shown for each matched peak). The peak assignment information shown here are for the 120 min time point from the Fe-EDTA-Rev/RRE RNA/coreactants reaction.

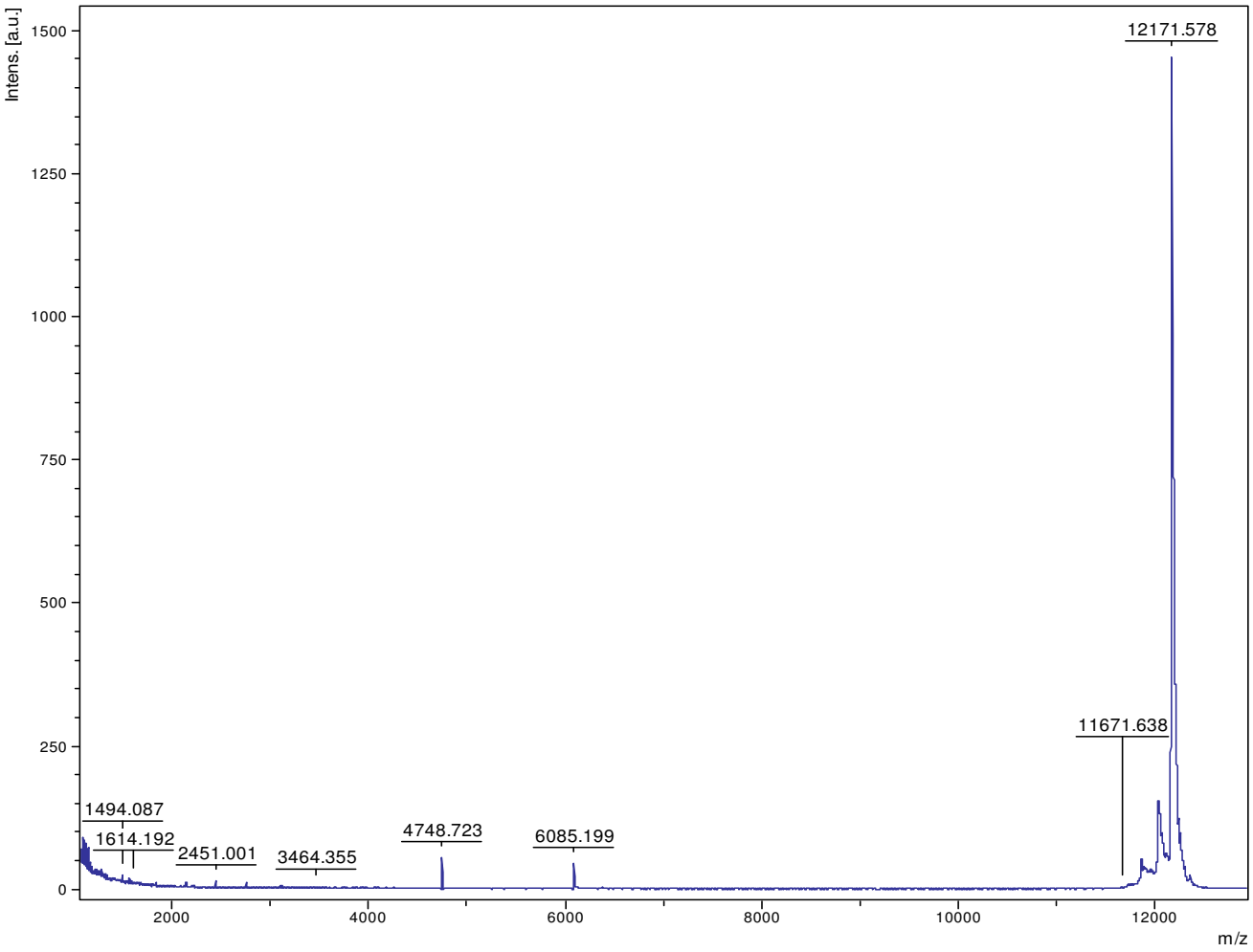

Figure SM1. MALDI-TOF mass spectrum for desalted mixture of Fl-RRE RNA, 1 mM H_2O_2, and 1 mM ascorbate, but lacking catalyst, after 1 h incubation at 37 ºC. The expected mass for the $[\text{Fl-RRE} - 1\text{H}]^{1-}$ anion is 12171.5 amu. Other peaks with lower m/z are regularly observed fragmentation and/or endonucleolysis products containing 2',3'-cyclic(PO_4) and 5'-OH overhangs (c-fragments and y-fragments, respectively). The peak at 6085.2 amu is the doubly charged $[\text{Fl-RRE} - 2\text{H}]^{2-}$ anion. The triply-charged and other multiply-charged anions were not observed. The mass spectrum for Fl-RRE in the absence of coreactants was similar to the spectrum shown here. No oxidative strand scission was observed in the absence of metal complex but in the presence of redox coreactants.

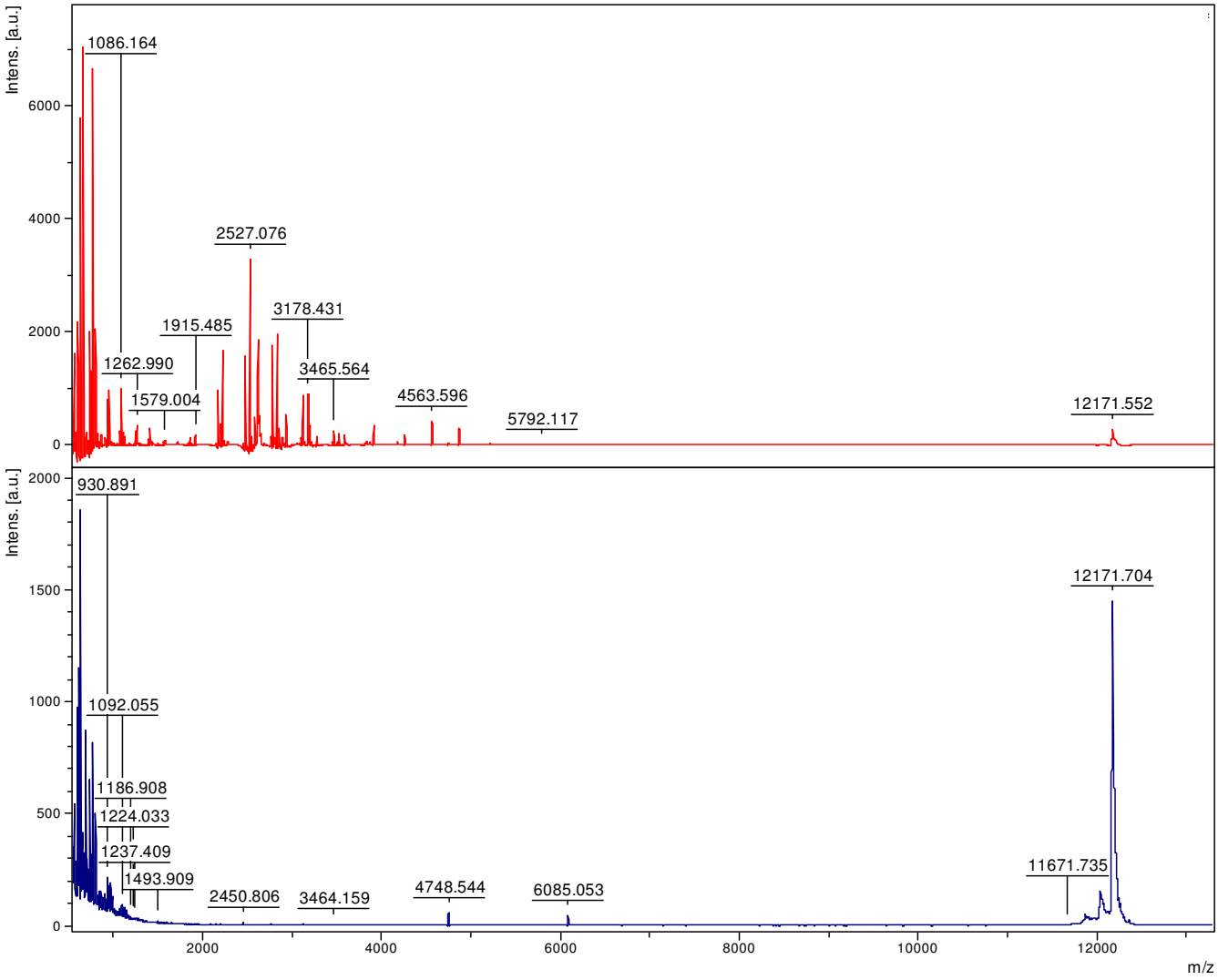

Figure SM2. Comparison of mass spectra for desalted mixtures of Fl-RRE RNA incubated for 1 h with coreactants (H_2O_2 and ascorbate) and with Fe-EDTA-Rev (red) vs without added catalyst (blue).

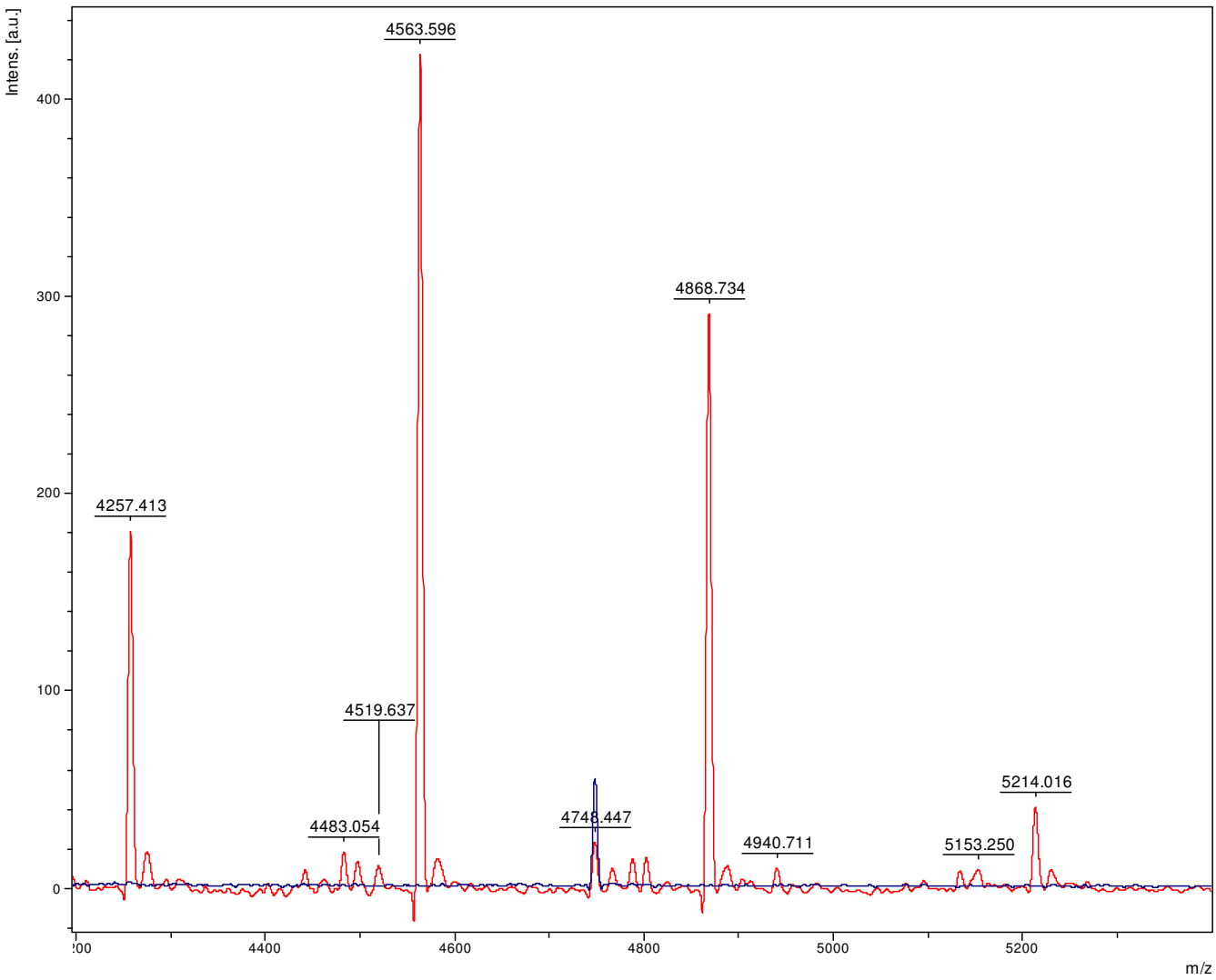

Figure SM2 (cont'd). Focus on the region 4200 to 5400 amu, showing that certain overhangs resulted only from catalyst-mediated cleavage, while other fragments that resulted from 2'-OH-mediated endonucleolytic pathways were observed even for the control reaction lacking catalyst. Note the blue peak at ~ 4748 amu, corresponding to the 5'-Fl-UUGGUCUGGGCGC-2',3'-c(PO_4) fragment.

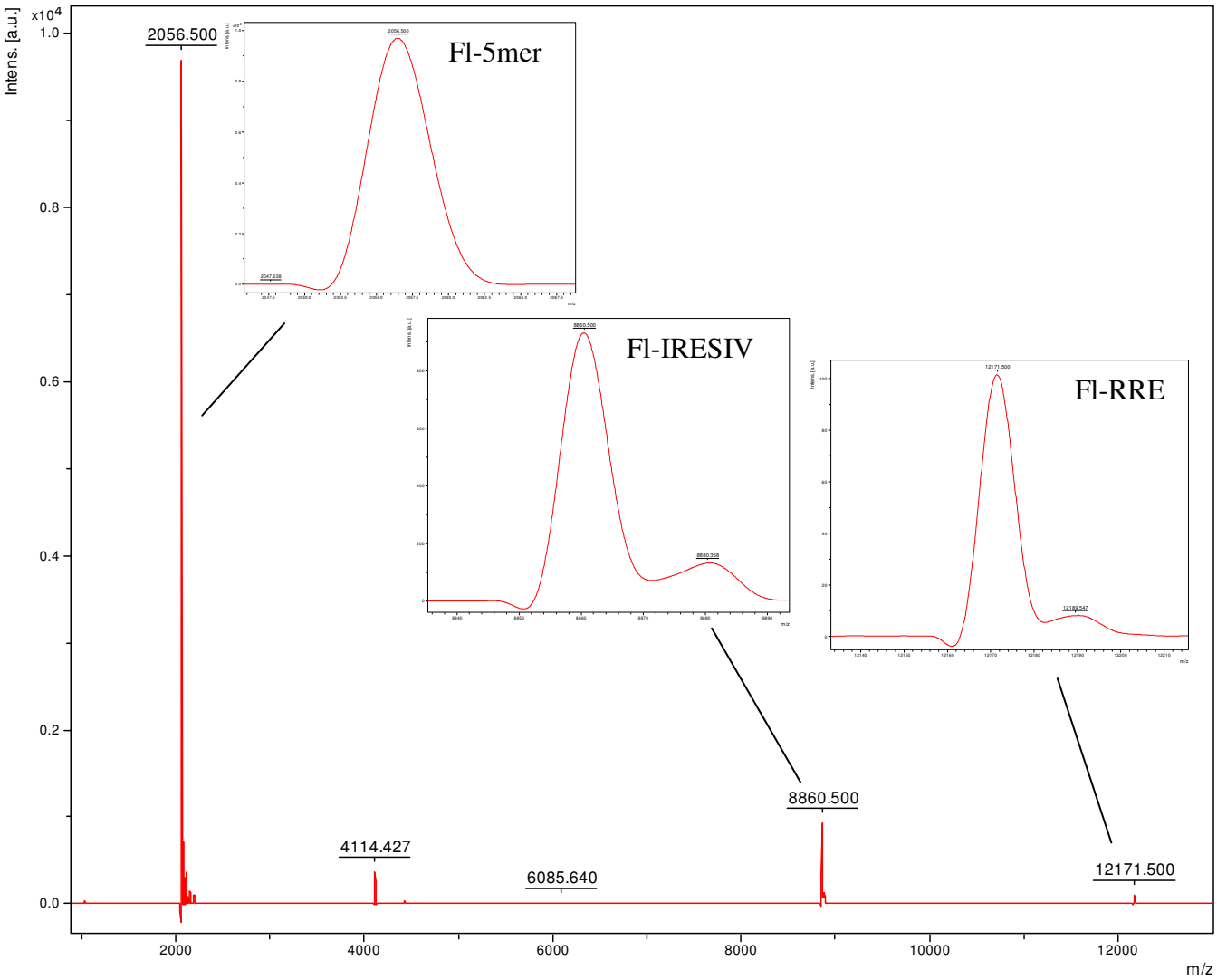

Figure SM3. Mixture of three RNA species used for mass calibration prior to each analysis: [Fl-RRE – 1H]$^{1-}$ (12171.5 amu), [Fl-IRESSLIV – 1H]$^{1-}$ (8850.5 amu), and [Fl-5-mer – 1H]$^{1-}$ (2056.5 amu). The mixture originally contained 10 µM of each RNA species in a buffer consisting of 20 mM HEPES, 100 mM NaCl, pH 7.4. This mixture was desalted by C_{18} ZipTip purification and analyzed by MALDI TOF MS (negative ion mode), as described in the manuscript. The total concentration of RNA bases in the original mixture was ~ 670 µM.

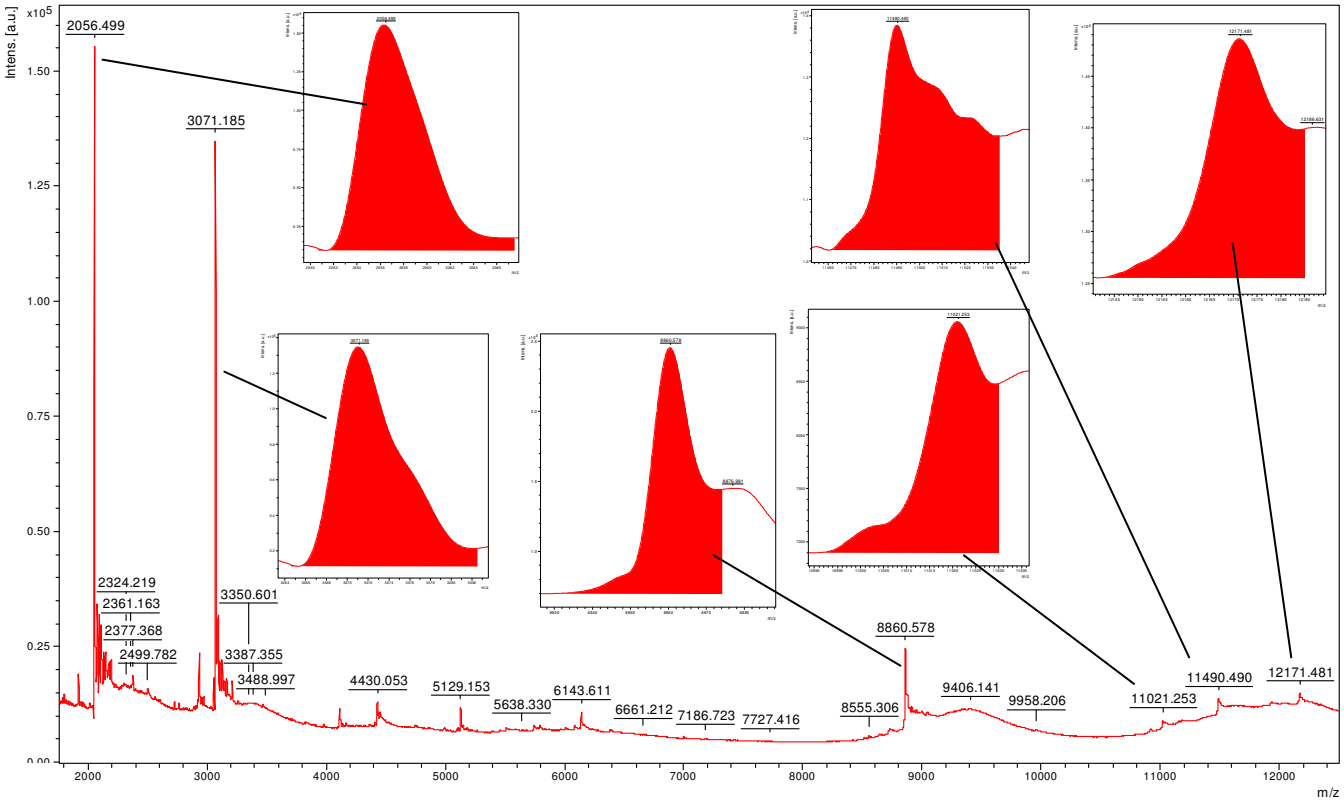

RNA Species	Observed m/z (amu)	Observed Peak Area
[Fl-5mer – 1H]$^{1-}$	2056.50	1094714
[Dylight547-8mer – 1H]$^{1-}$	3071.19	1119419
[Fl-IRESSLIV – 1H]$^{1-}$	8860.58	604009
[unlabelled RRE-1H]$^{1-}$	11021.25	319214
[Fl-SLIIB-1H]$^{1-}$	11490.49	912910
[Fl-RRE – 1H]$^{1-}$	12171.48	585082

Figure SM4. Mass bias. A mixture of six different RNA species with a range of masses (shown above), each originally present at 2.5 µM in 20 mM HEPES, 100 mM NaCl, pH 7.4, was desalted by C_{18} ZipTip purification and analyzed by MALDI-TOF MS, as described in the manuscript. Detection of RNA fragments was biased toward fragments with smaller mass, as shown in the table above, and this skewing of the apparent abundances in favor of species with lower mass appeared to result from the desalting and/or MALDI TOF processes. Note that the peak width increases for RNA with higher m/z (peak area is more accurate than peak height for quantification). The total concentration of RNA bases in the original mixture was ~ 360 µM, the same as used in experiments involving cleavage of Fl-RRE RNA (10 µM of the 36mer).

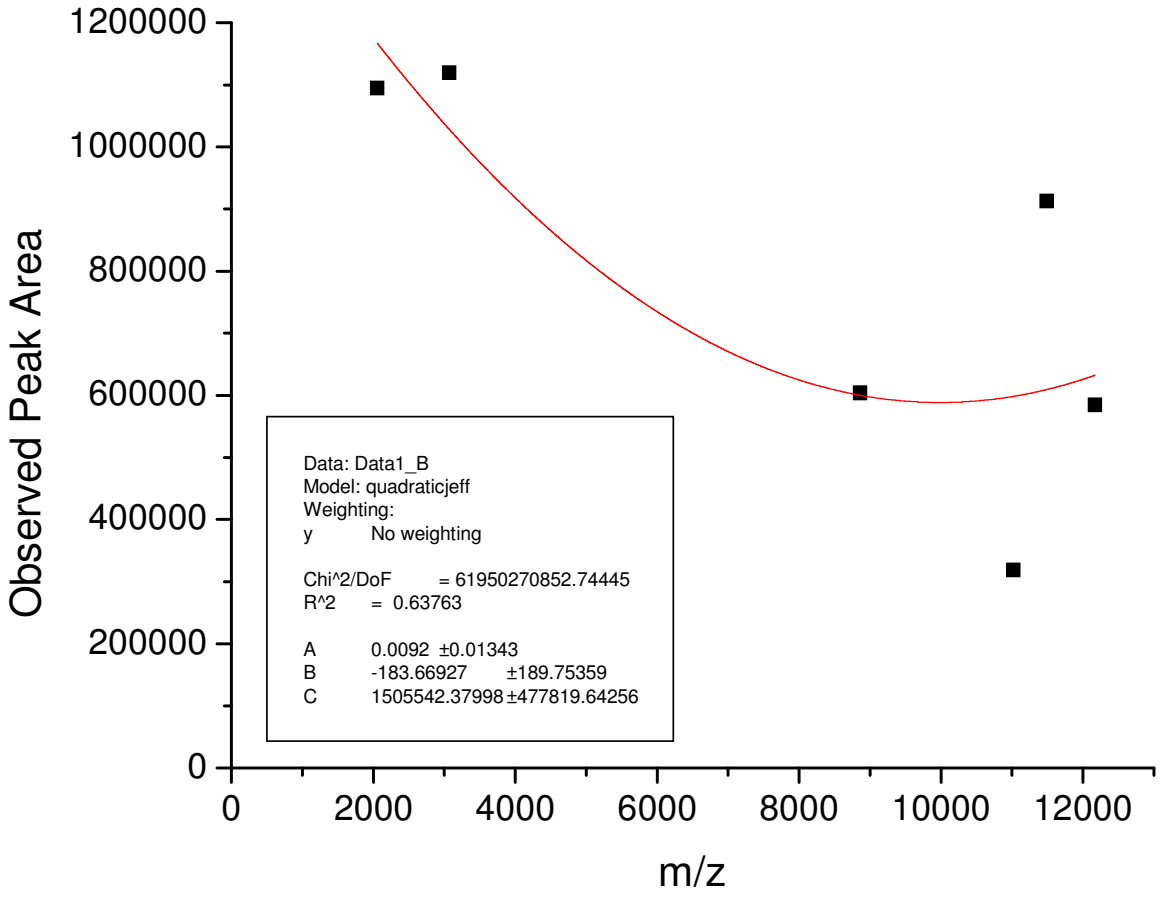

Figure SM5. Mass bias. For the mass spectrum shown in Figure SM4, which includes a mixture of six different RNA species with a range of masses, the observed peak areas were plotted vs the m/z. The plot was fit to a parabola, the fitted parameters of which would allow for external calibrations of the peak areas in mass spectra if errors on the fitted parameters were sufficiently low, prior to conversion of peak areas to peak area fractions. External calibrations of peak areas were not performed for any of the data shown in the manuscript or the Supporting Information.

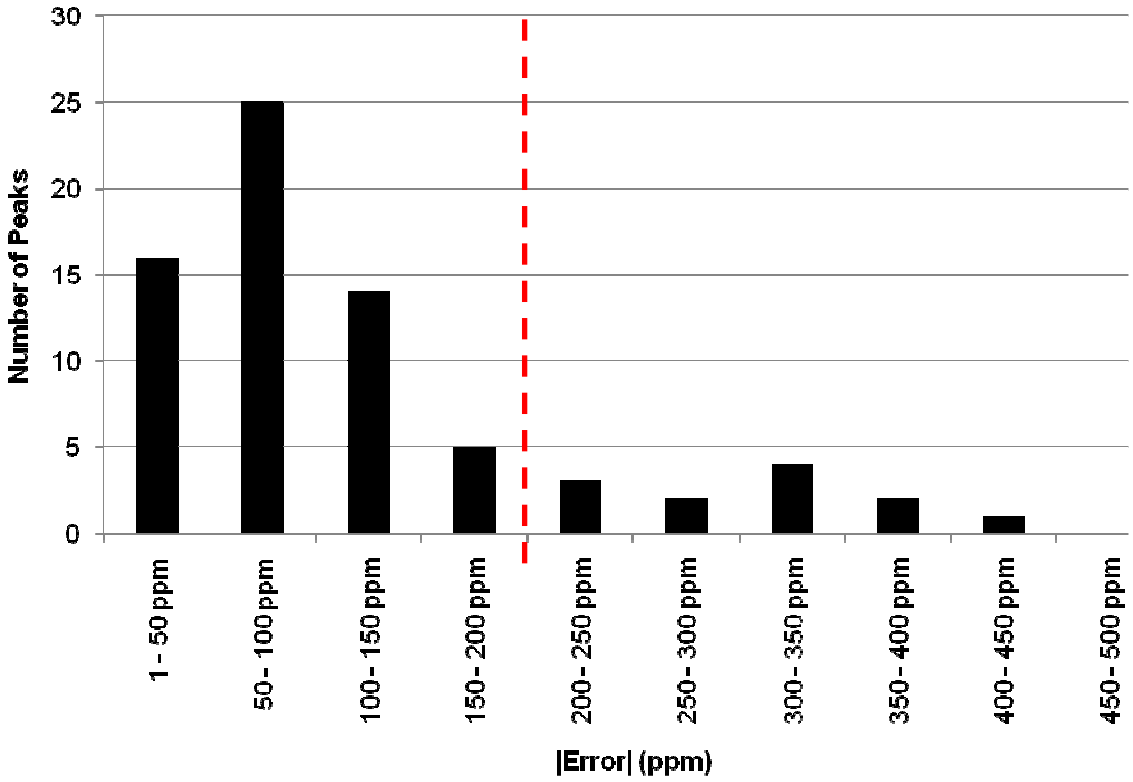

Figure SM6. Histogram showing the distribution of mass-matching errors for all assigned peaks for one reaction. Although a mass-matching tolerance of 200 ppm was used for all other data (shown by the red dashed line), the data shown in this figure were generated by use of a mass-matching tolerance of 500 ppm, in order to show the distribution of errors. When a mass-matching tolerance of 200 ppm was used, the root-mean-square (RMS) mass-matching error for the reaction was 113 ppm. The data and RMS calculation shown here are from the 120 min time point from the Fe-EDTA-Rev/RRE RNA/coreactants reaction.

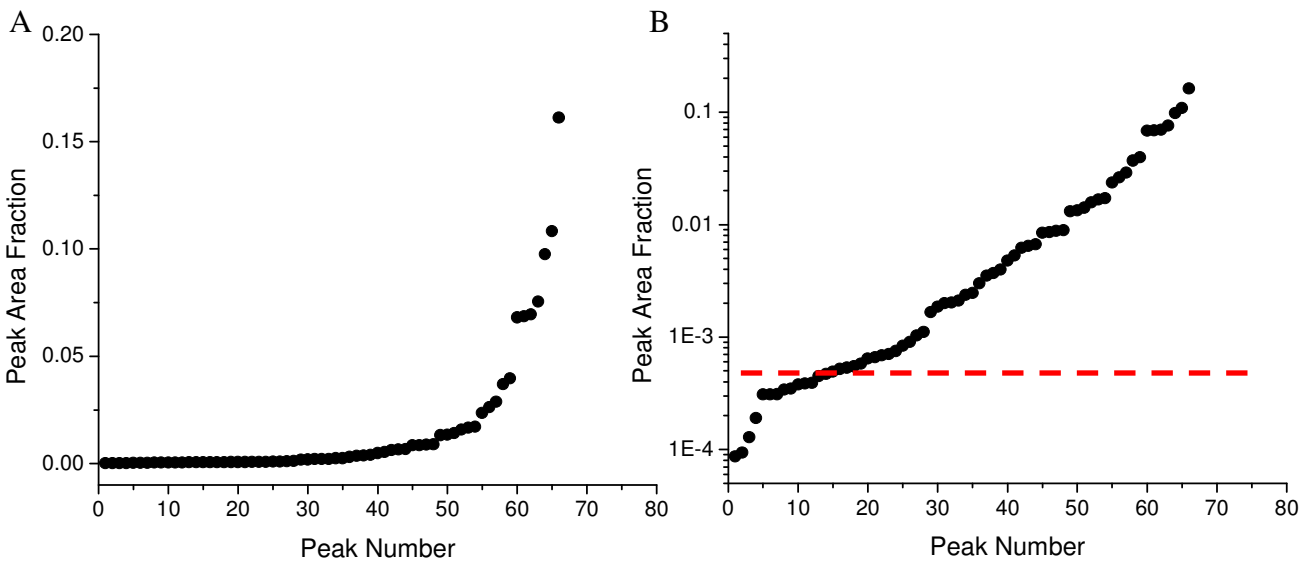

Figure SM7. In order for a MS peak to be considered 'real', the peak area fraction was required to be >0.0005, following assignment of peaks. Additionally, the m/z for an observed peak was required to be within a matching threshold (200 ppm) relative to the m/z for the predicted peak (shown elsewhere). The peaks shown here resulted from the 120 min timepoint from the Fe-EDTA-Rev/RRE RNA/coreactants reaction: (A) linear plot and (B) semi-log plot of the same data. The peak area fraction threshold of 0.0005 is represented by the red line.

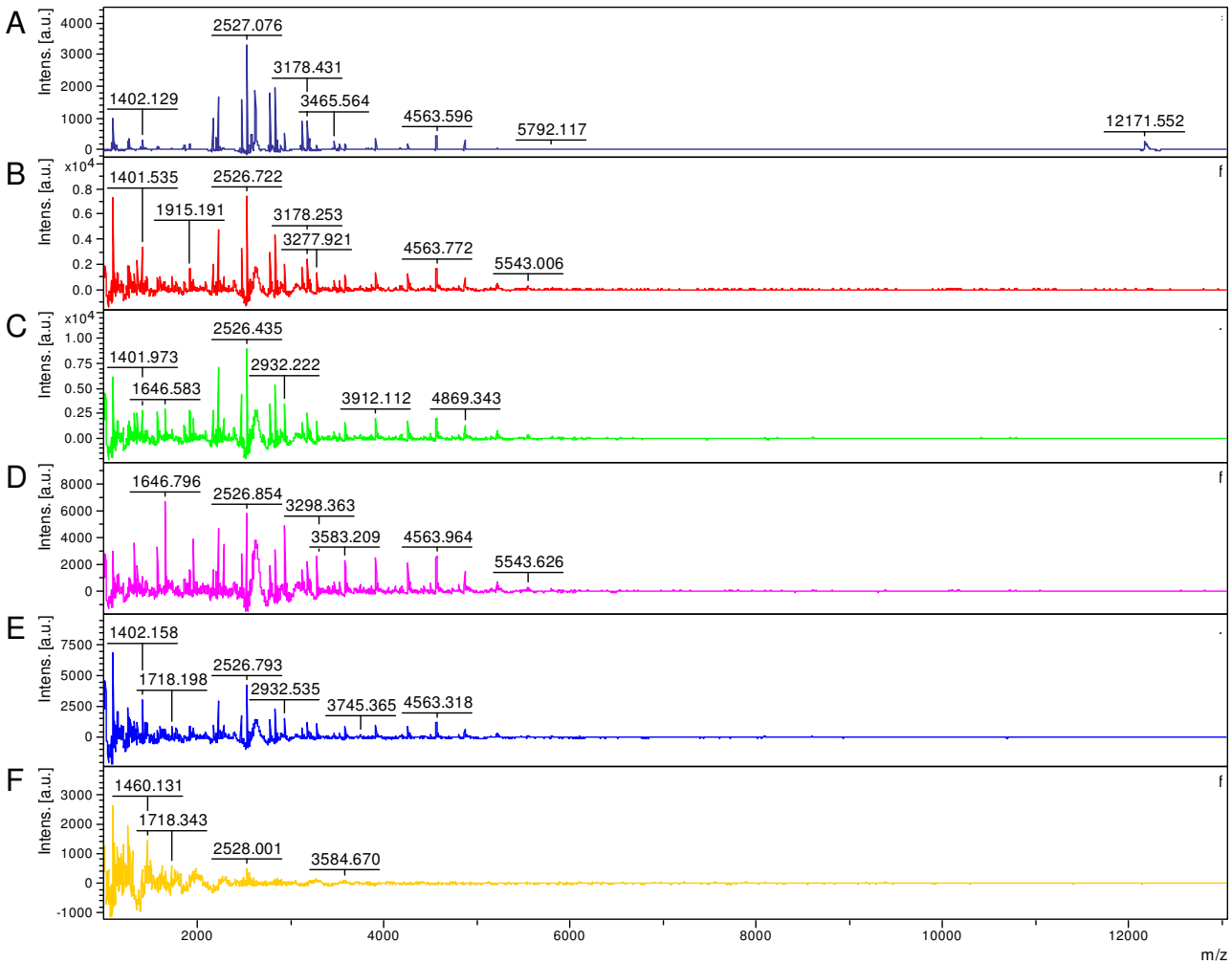

Figure SM8. Comparison of sample washing procedures for the C_{18} ZipTip desalting protocol, following loading of the RNA samples onto the ZipTip, but prior to elution of RNA. Samples contained a reaction mixture following a 1h incubation of 10 µM Fl-RRE RNA with 10 µM Fe-EDTA-Rev and 1 mM H_2O_2 + ascorbate. Samples were washed as follows: (A) with three 10 µL volumes of 2M triethylamine acetate (TEAA) buffer, then three 10 µL volumes of H_2O; (B) with two 10 µL volumes of 2M TEAA buffer, then three 10 µL volumes of H_2O; (C) with one 10 µL volume of 2M TEAA buffer, then three 10 µL volumes of H_2O; (D) only three 10 µL volumes of H_2O; (E) with one 10 µL volume of 2M TEAA buffer, then one 10 µL volume of H_2O; (F) with three 10 µL volumes of 2M TEAA buffer only (no washing with H_2O). Moving from (A) through (D), the number of sequential washings with 2M TEAA buffer is decreased sequentially from three to zero, and two observations can be made: (1) the abundance of low-mass peaks (~2000 amu) increases as the number of washes with 2M TEAA buffer decreases, suggesting some loss of lower MW products when washing with 2M TEAA; (2) the apparent abundance of 3' fragments increases, relative to 5'-fluorescein labeled fragments, as the number of washes with 2M TEAA buffer decreases, suggesting greater loss of non-labeled fragments, which are less hydrophobic, during washes with 2M TEAA. The lack of peaks observed in (F) demonstrates the necessity of washing with H_2O (compare with (A)).

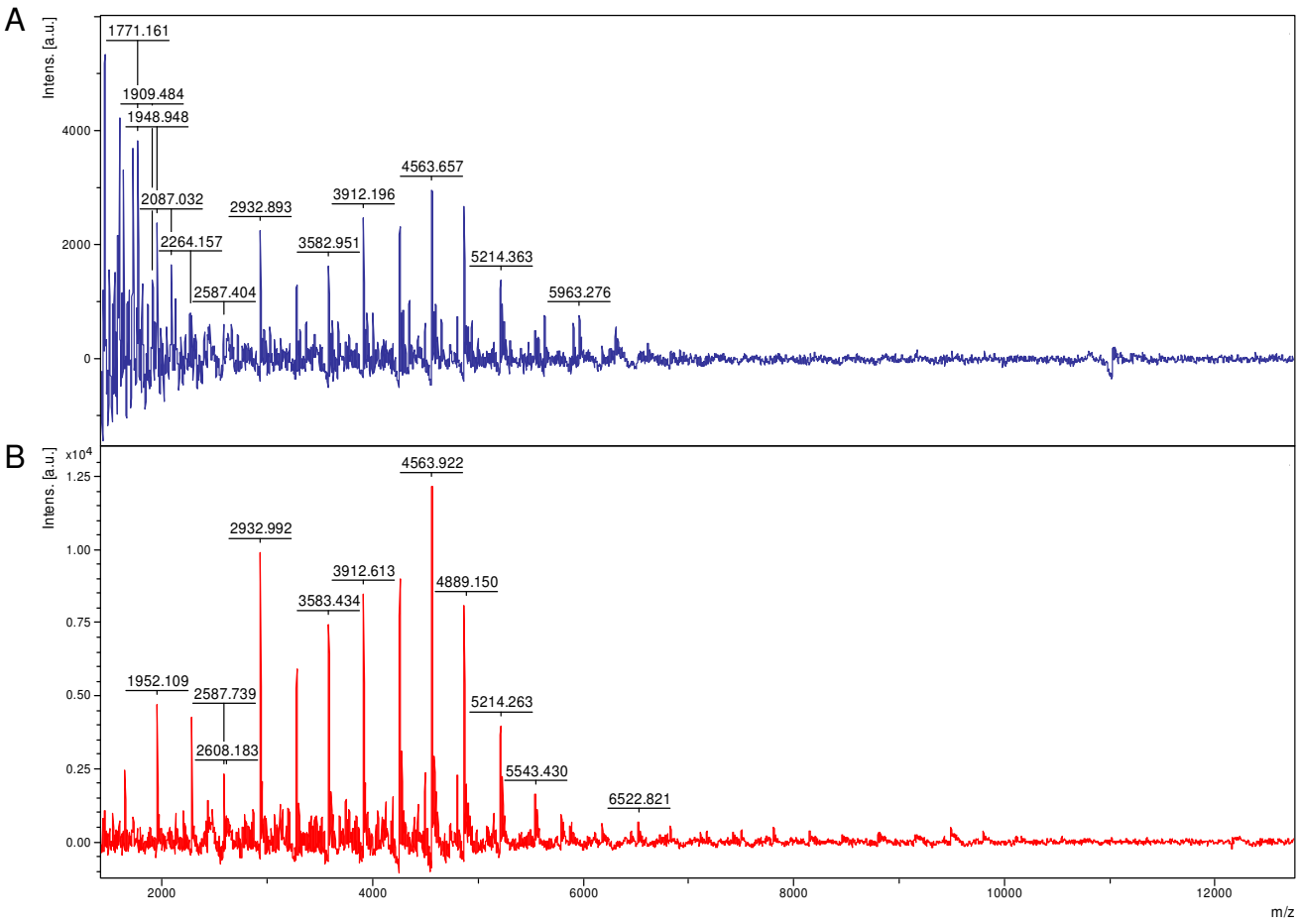

Figure SM9. Ethanol precipitation as the desalting method. (A) unlabelled RRE RNA (34mer) and (B) Fl-RRE RNA. Catalyst Fe-EDTA-Rev (10 μM) and H_2O_2/ascorbate (1 mM) were incubated for 1 h with either (A) 10 μM unlabelled RRE RNA (34mer) or (B) Fl-RRE RNA (36mer). Following reaction, samples were quenched and desalted as described by McKenzie et al (2012).[1]

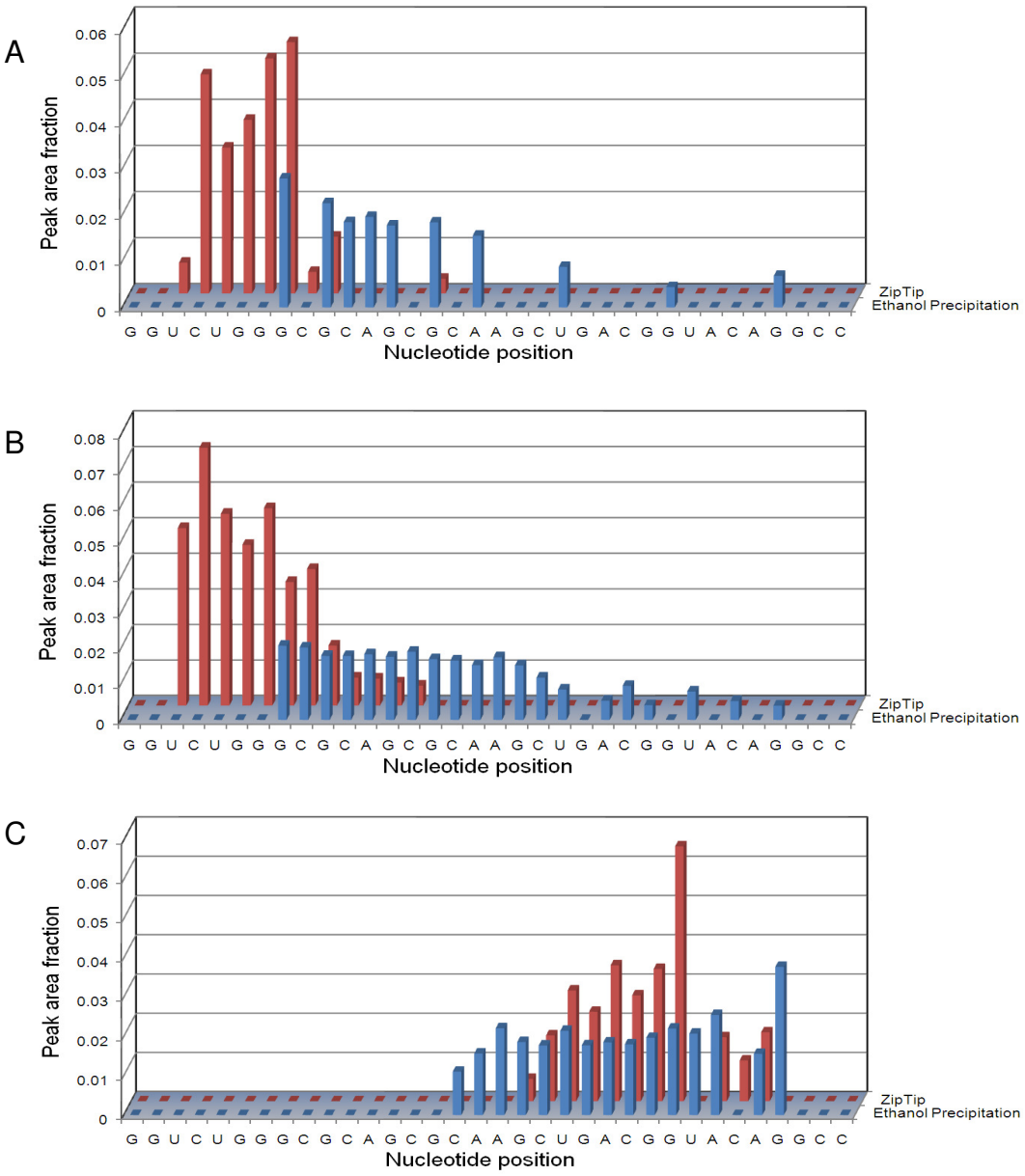

Figure SM10. Ethanol precipitation (front/blue) vs ZipTip desalting (rear/red). Catalyst Fe-EDTA-Rev (10 μM) and H_2O_2/ascorbate (1 mM) were incubated for 1 h with 10 μM unlabelled RRE RNA (34mer), and the peak area fractions of all products were determined. (A) RNA cleavage fragments containing nascent terminal 3'-phosphates; (B) cleavage fragments containing nascent terminal 3'-phosphoglycolates; (C) cleavage fragments containing nascent terminal 5'-phosphates. Ethanol precipitation allowed identification of some larger RNA fragments that were not recovered following the ZipTip protocol. However, many of the smaller RNA fragments that were observed following the ZipTip protocol were lost during ethanol precipitation, as expected. The loss of lower-mass fragments could explain the higher peak area fractions for higher-mass fragments, that are seen for the ethanol precipitation method. Ethanol precipitation was performed as described by McKenzie et al (2012).[1]

Before Base	Average % of fragmentation products
A	50 ± 40
U	20 ± 30
G	30 ± 40
C	6 ± 7
After Base	Average % of fragmentation products
A	4 ± 7
U	5 ± 7
G	30 ± 30
C	60 ± 40

Table SM5. Occurrence of background fragmentation, relative to base composition. The % abundance of fragmentation products containing nascent 2',3'-cyclic phosphates resulting from fragmentation either before or after each base, were determined for Fl-16S RNA (at time zero in incubations with several catalysts and co-reactants). No significant dependence of fragmentation on base composition was observed.

Before Base	Average % of fragmentation products
A	10 ± 20
U	10 ± 20
G	50 ± 30
C	20 ± 30
After Base	Average % of fragmentation products
A	1 ± 2
U	40 ± 30
G	40 ± 30
C	20 ± 30

Table SM6. Occurrence of background fragmentation, relative to base composition. The % abundance of fragmentation products containing nascent 2',3'-cyclic phosphates resulting from fragmentation either before or after each base, were determined for Fl-RRE RNA (at time zero in incubations with several catalysts and co-reactants). No significant dependence of fragmentation on base composition was observed.

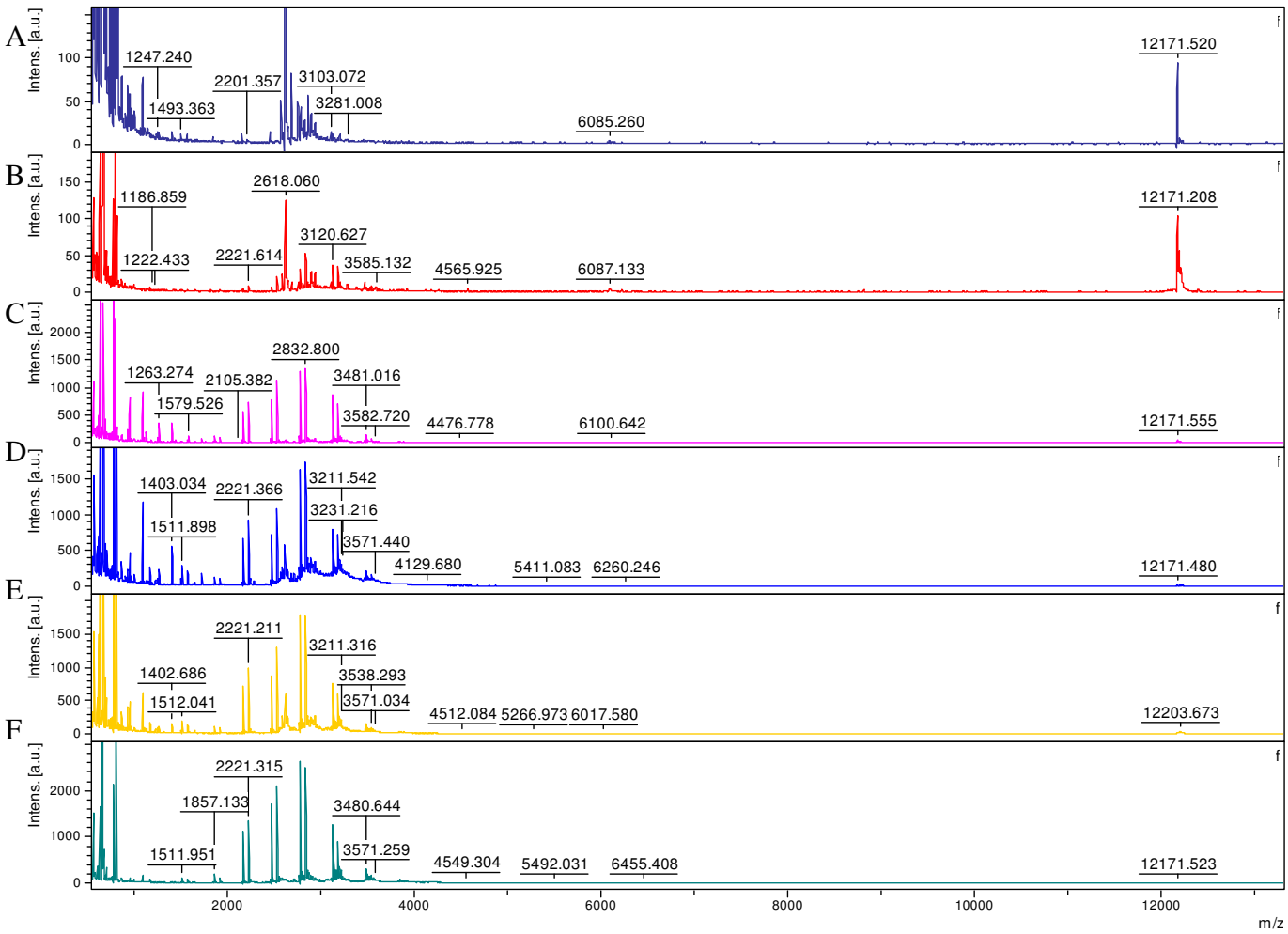

Figure SM11. MALDI-TOF mass spectra for time-dependent incubations of 10 µM Cu-NTA-Rev, 1 mM H_2O_2/ascorbate, and 10 µM Fl-RRE RNA at 37 ºC. (A) 0 min; (B) 2 min; (C) 7 min; (D) 10 min; (E) 20 min; (F) 30 min.

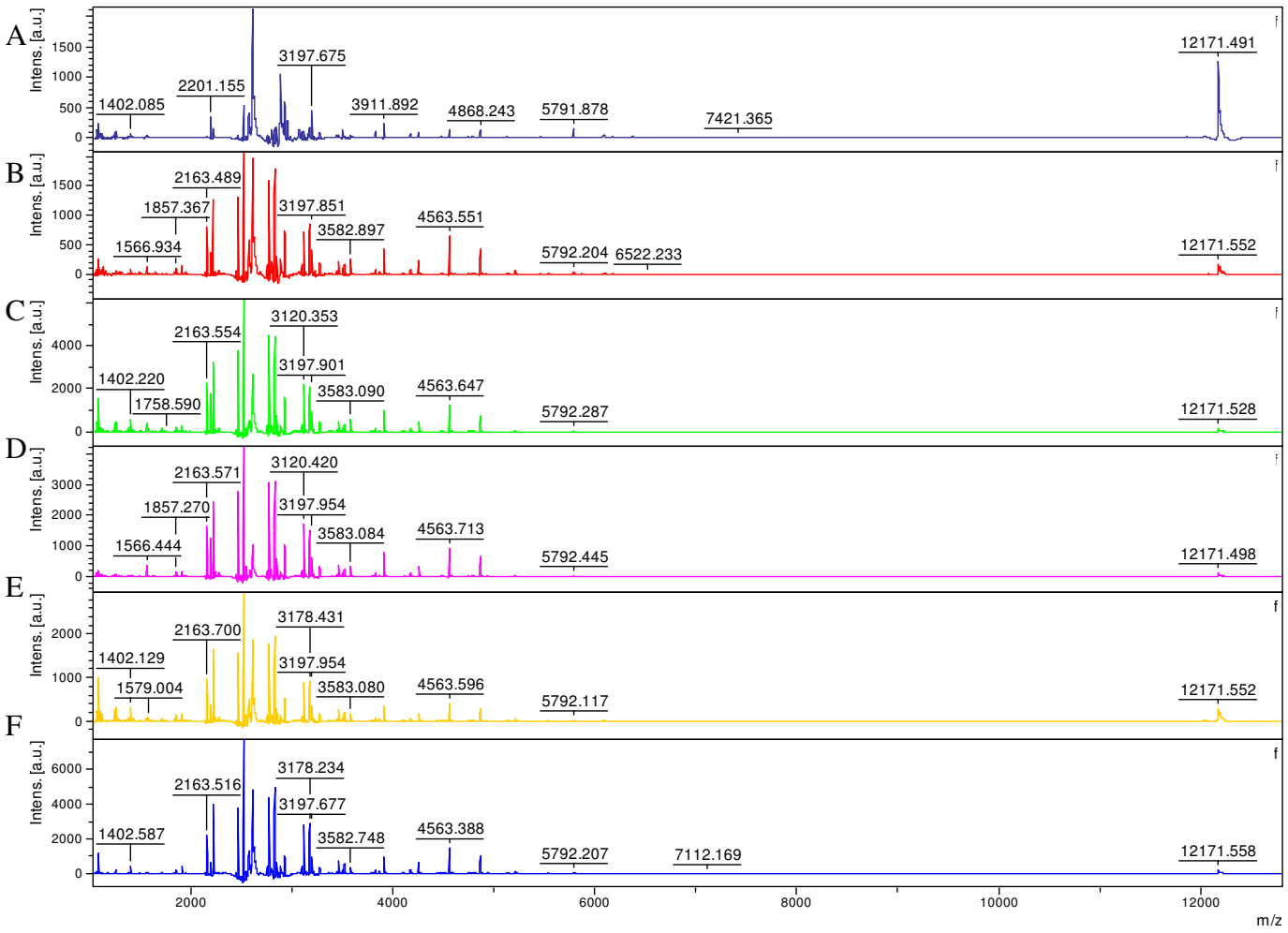

Figure SM12. MALDI-TOF mass spectra for time-dependent incubations of 10 µM Fe-EDTA-Rev, 1 mM H_2O_2/ascorbate, and 10 µM Fl-RRE RNA at 37 ℃. (A) 0 min; (B) 2 min; (C) 5 min; (D) 10 min; (E) 60 min; (F) 120 min.

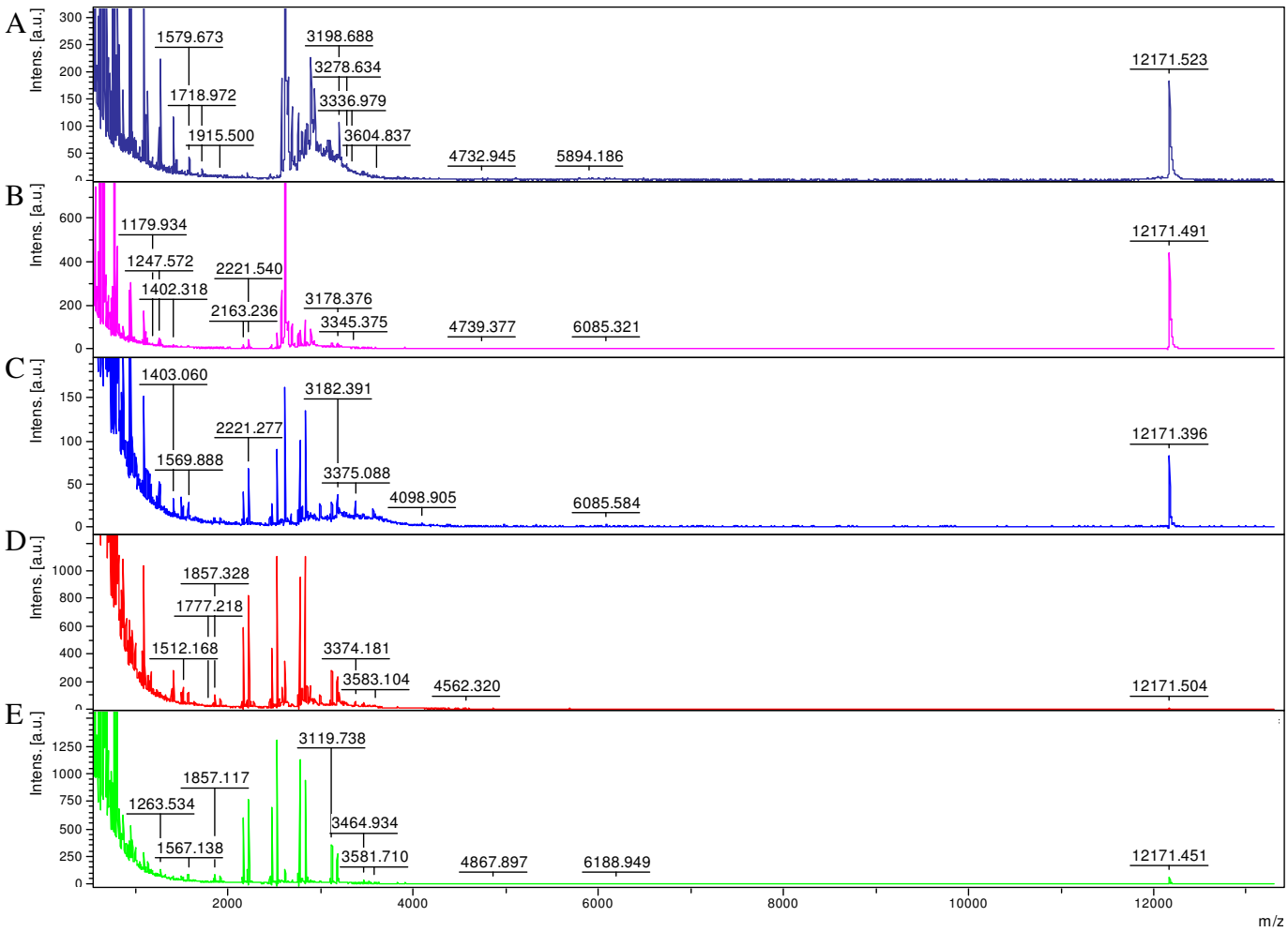

Figure SM13. MALDI-TOF mass spectra for time-dependent incubations of 10 µM Fe-NTA-Rev, 1 mM H_2O_2/ascorbate, and 10 µM Fl-RRE RNA at 37 ºC. (A) 0 min; (B) 5 min; (C) 10 min; (D) 30 min; (E) 45 min.

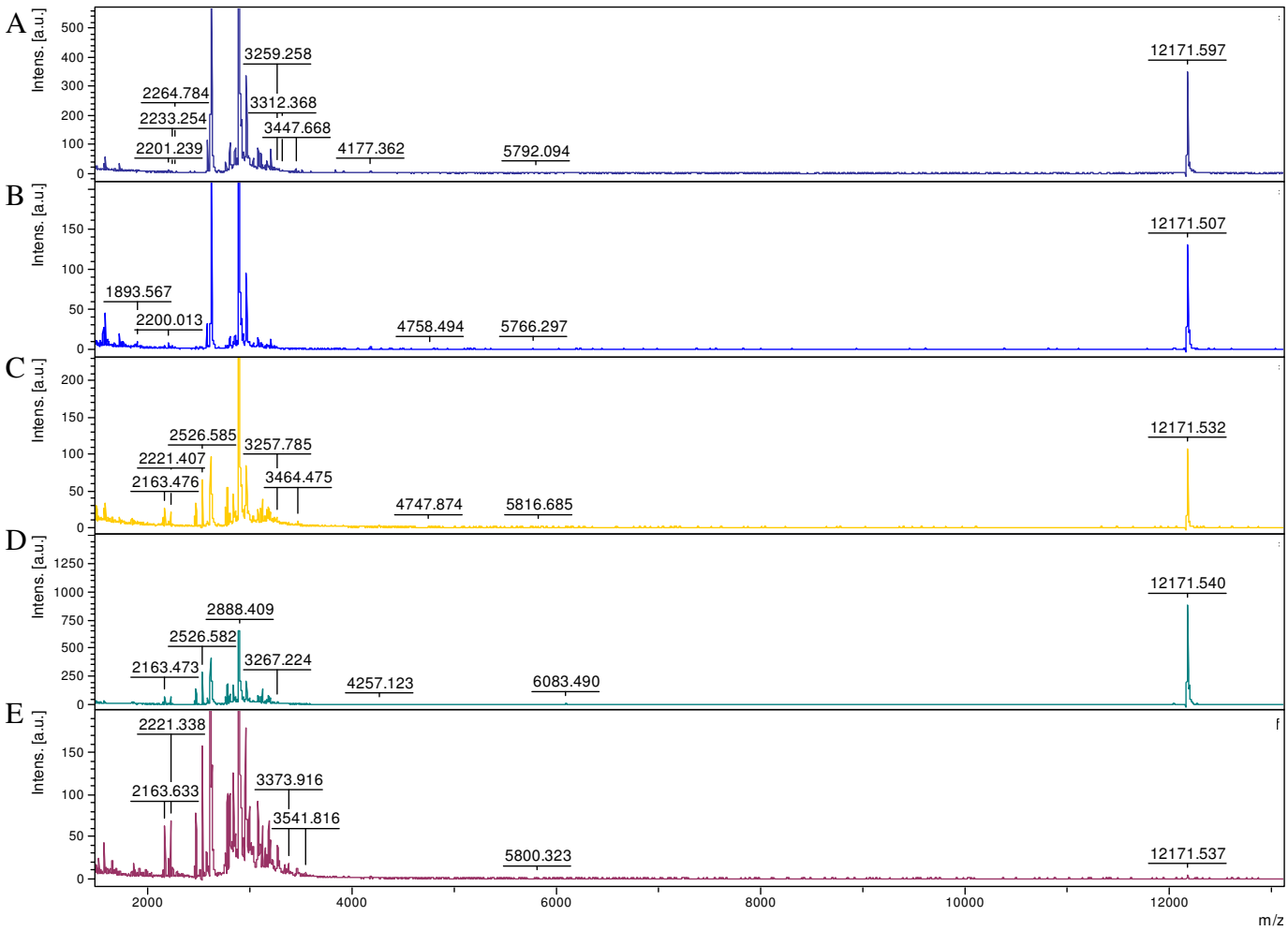

Figure SM14. MALDI-TOF mass spectra for time-dependent incubations of 10 µM Cu-EDTA-Rev, 1 mM H_2O_2/ascorbate, and 10 µM Fl-RRE RNA at 37 ºC. (A) 0 min; (B) 10 min; (C) 20 min; (D) 30 min; (E) 45 min.

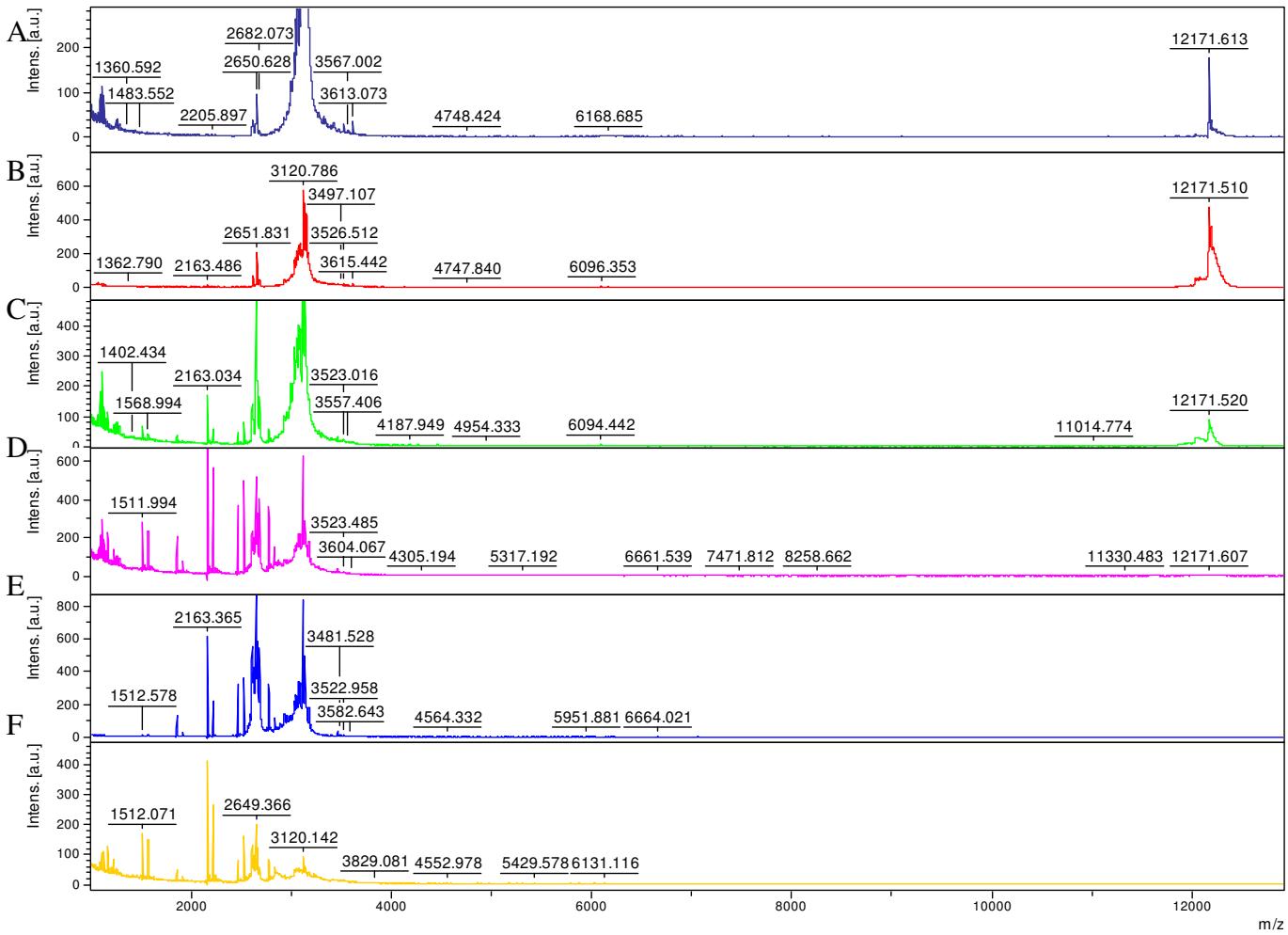

Figure SM15. MALDI-TOF mass spectra for time-dependent incubations of 10 µM Fe-DTPA-Rev, 1 mM H_2O_2/ascorbate, and 10 µM Fl-RRE RNA at 37 ºC. (A) 0 min; (B) 30 min; (C) 60 min; (D) 90 min; (E) 120 min; (F) 180 min.

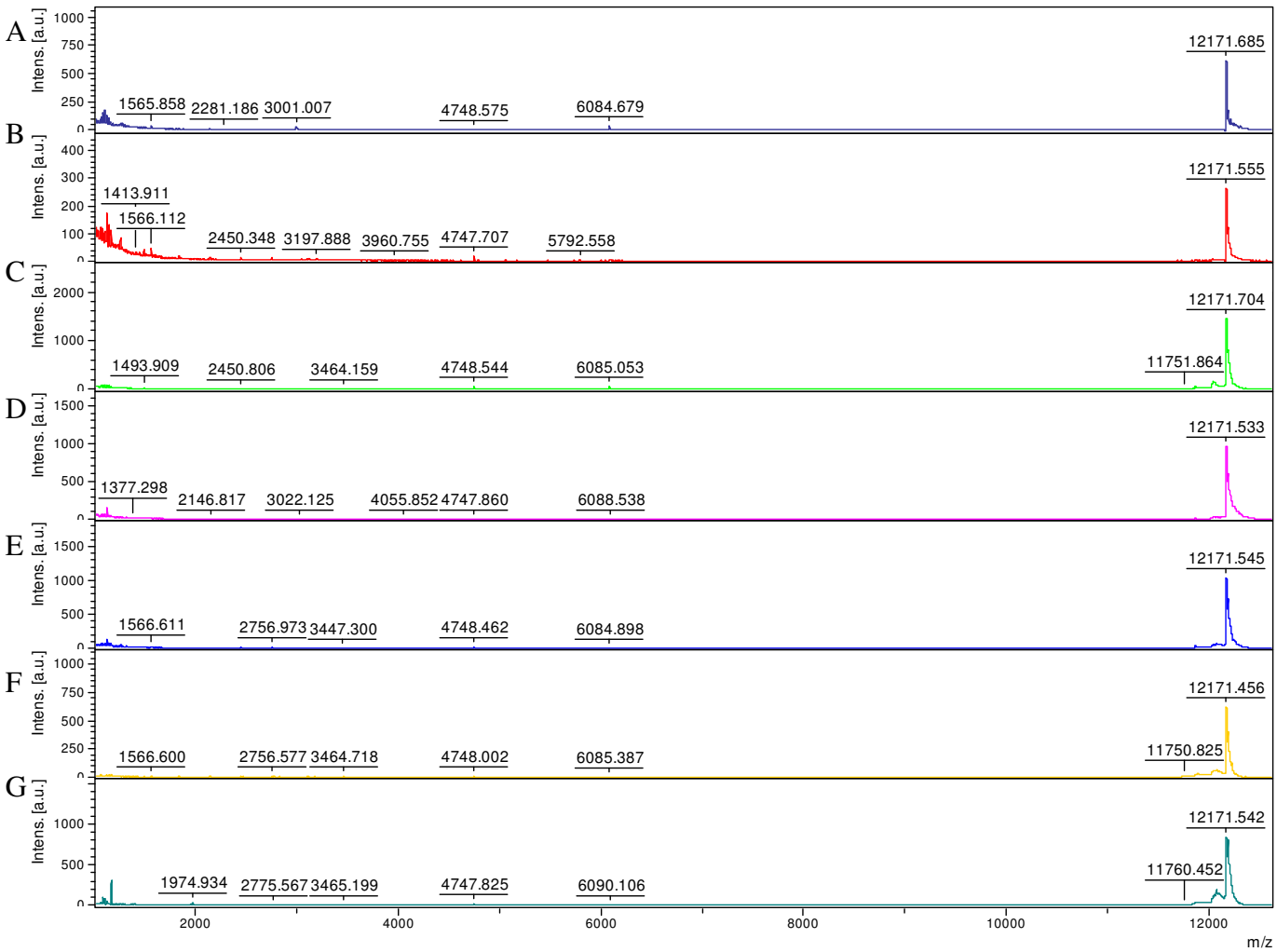

Figure SM16. MALDI-TOF mass spectra for time-dependent incubations of 1 mM H_2O_2/ascorbate (no catalyst), and 10 µM Fl-RRE RNA at 37 ºC. (A) 0 min; (B) 30 min; (C) 60 min; (D) 90 min; (E) 120 min; (F) 150 min; (G) 180 min.

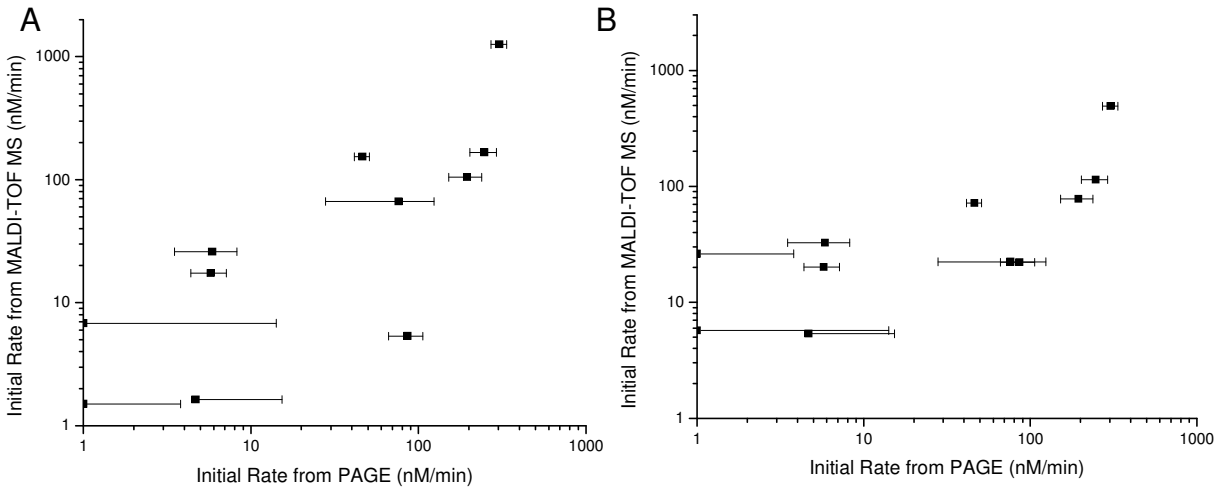

Figure SM17. Comparison of MALDI-TOF MS vs 5'-fluorescein-monitored PAGE analysis for time-dependent cleavage of Fl-RRE RNA by various ribonuclease mimics (a similar analysis to that shown for Fl-16S RNA in the main text). For MALDI-TOF MS, initial rates of cleavage were obtained for a series of reactions by use of either (A) method 1 or (B) method 2 (y-axes of A and B). For PAGE analysis, initial rates were obtained for the same reactions as the rate of disappearance of full-length RNA (x-axes of A and B). For Fl-RRE RNA (12172.5 Da), the rates were generally within ~6-fold agreement between the MALDI-TOF MS and PAGE assays (with only one exeption for either method). For Fl-16S RNA (9176.7 Da), the rates were generally within ~2-fold agreement between the MALDI-TOF MS and PAGE assays. The decrease in accuracy of the MALDI-TOF MS method for Fl-RRE RNA, relative to the smaller Fl-16S RNA, most likely reflects mass bias effects of the MALDI-TOF MS method.

catalyst	Apparent Initial Rate of RNA Modification (nM/min)			
	MALDI method 1	MALDI method 2	PAGE	AP-RNA [a]
Fe-EDTA-Rev	1100	500	4000 ± 1000	5200 ± 100
Cu-NTA-Rev	1300	500	300 ± 30	1400 ± 100
Fe-NTA-Rev	200	100	250 ± 40	3200 ± 100
Cu-EDTA-Rev	200	70	46 ± 5	~ 0
Fe-DTPA-Rev	100	80	190 ± 40	n.d.
Co-NTA-Rev	26	30	6 ± 2	640 ± 20
Ni-NTA-Rev	10	20	90 ± 20	n.d.
Co-EDTA-Rev	18	20	6 ± 1	0 ± 1
Co-KGHK-Rev	10	6	< 11	n.d.
Ni-KGHK-Rev	2	5	< 15	n.d.
Cu-KGHK-Rev	70	20	80 ± 50	n.d.
None	2	30	1 ± 3	4.0 ± 0.5

Table SM7. Comparison of MALDI-TOF MS, PAGE, and fluorimetry (AP-RNA) assays for quantification of the initial rate of modification of RRE RNA. Reactions contained 10 μM RNA (Fl-RRE RNA for MALDI and PAGE; AP-RNA for the fluorimetry assay), 1 mM H_2O_2/ascorbate, and 10 μM catalyst (if present). [a] The AP-RNA construct corresponds to RRE RNA with an internal 2-aminopurine, the fluorescence of which decreases upon a conformational change in the RNA, following reaction; rates for the AP-RNA assay tend to be higher than for the PAGE assay, due to differences in what is being monitored, as described previously.[2]

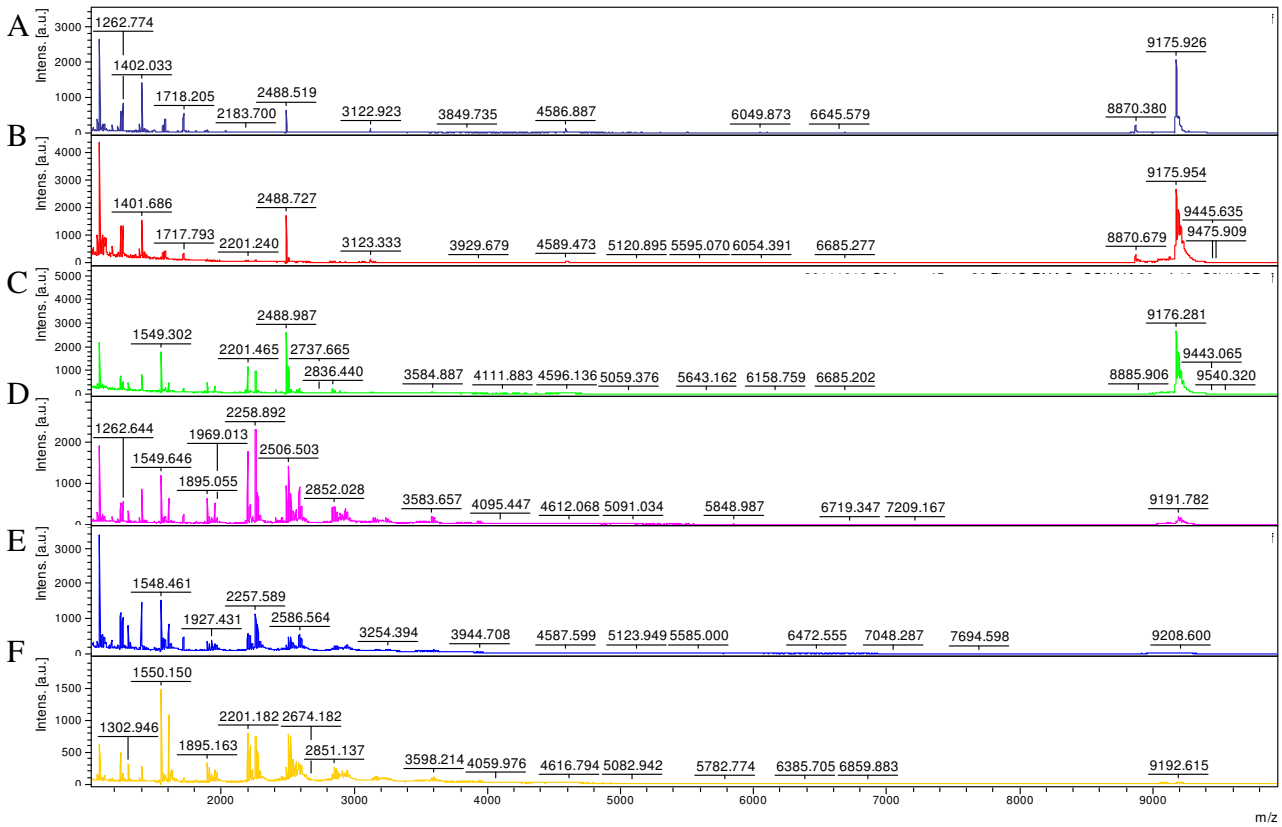

Figure SM18. MALDI-TOF mass spectra for time-dependent incubations of 10 µM Cu-GGH, 1 mM H_2O_2/ascorbate, and 10 µM Fl-16S RNA at 37 ºC. (A) 0 min; (B) 15 min; (C) 30 min; (D) 60 min; (E) 90 min; (F) 120 min.

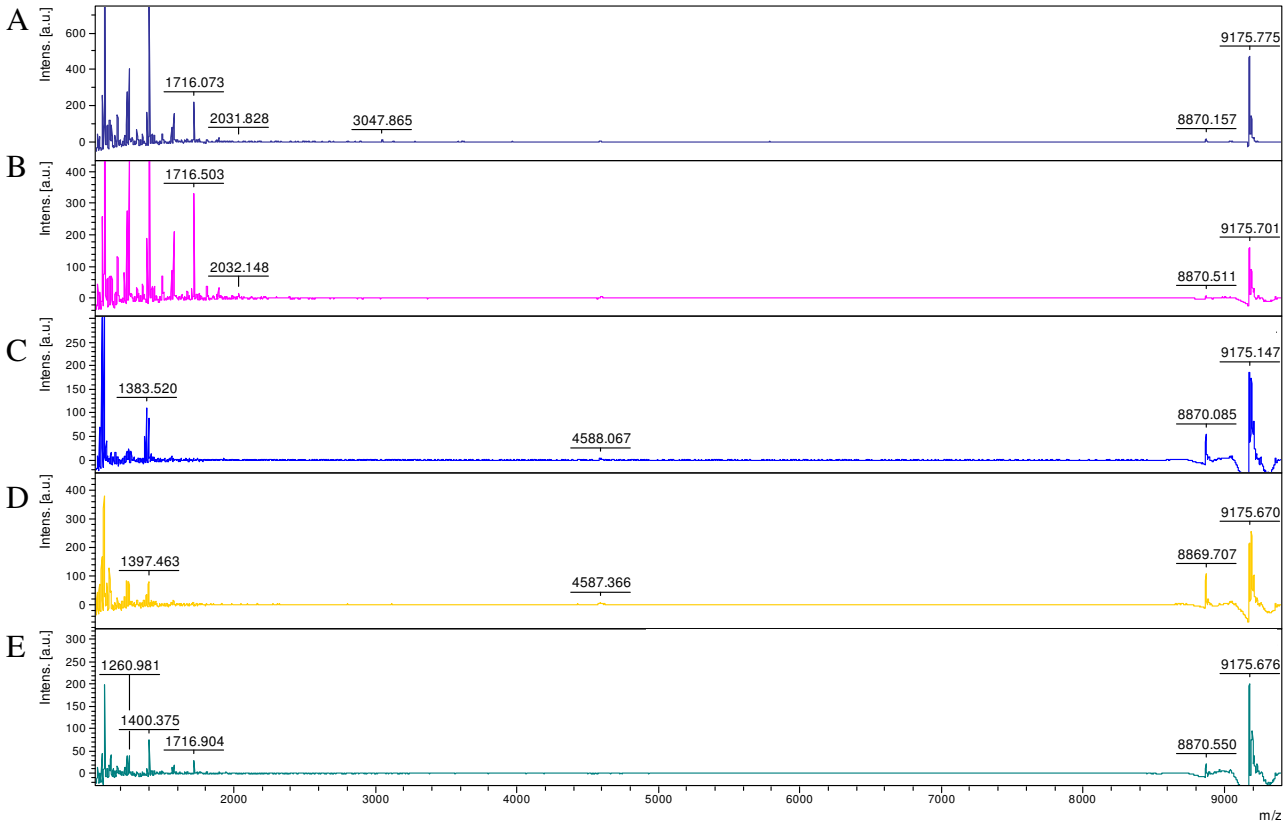

Figure SM19. MALDI-TOF mass spectra for time-dependent incubations of 1 mM H_2O_2/ascorbate (no catalyst), and 10 µM Fl-16S RNA at 37 ºC. (A) 0 min; (B) 30 min; (C) 40 min; (D) 90 min; (E) 120 min.

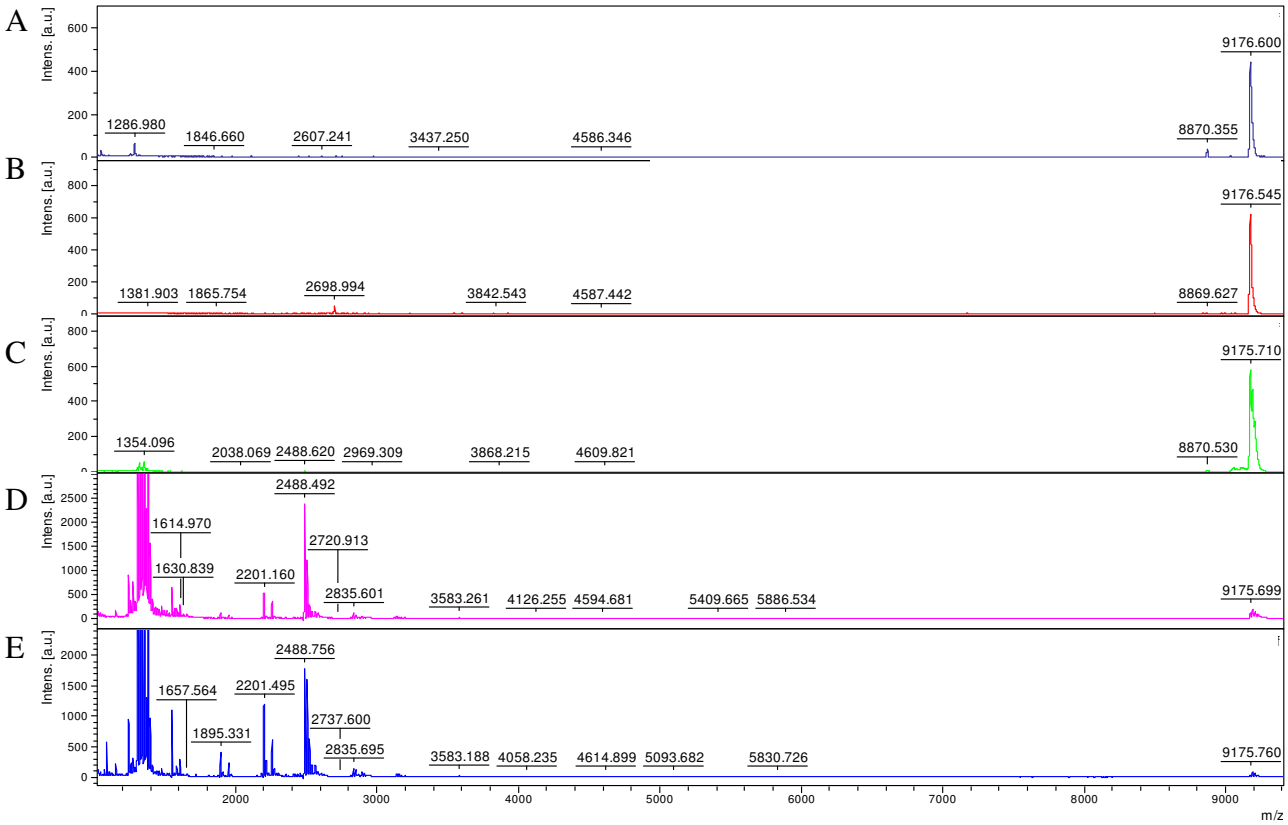

Figure SM20. MALDI-TOF mass spectra for time-dependent incubations of 10 µM Cu-PEP204, 1 mM H_2O_2/ascorbate, and 10 µM Fl-16S RNA at 37 ºC. (A) 0 min; (B) 10 min; (C) 40 min; (D) 90 min; (E) 120 min.

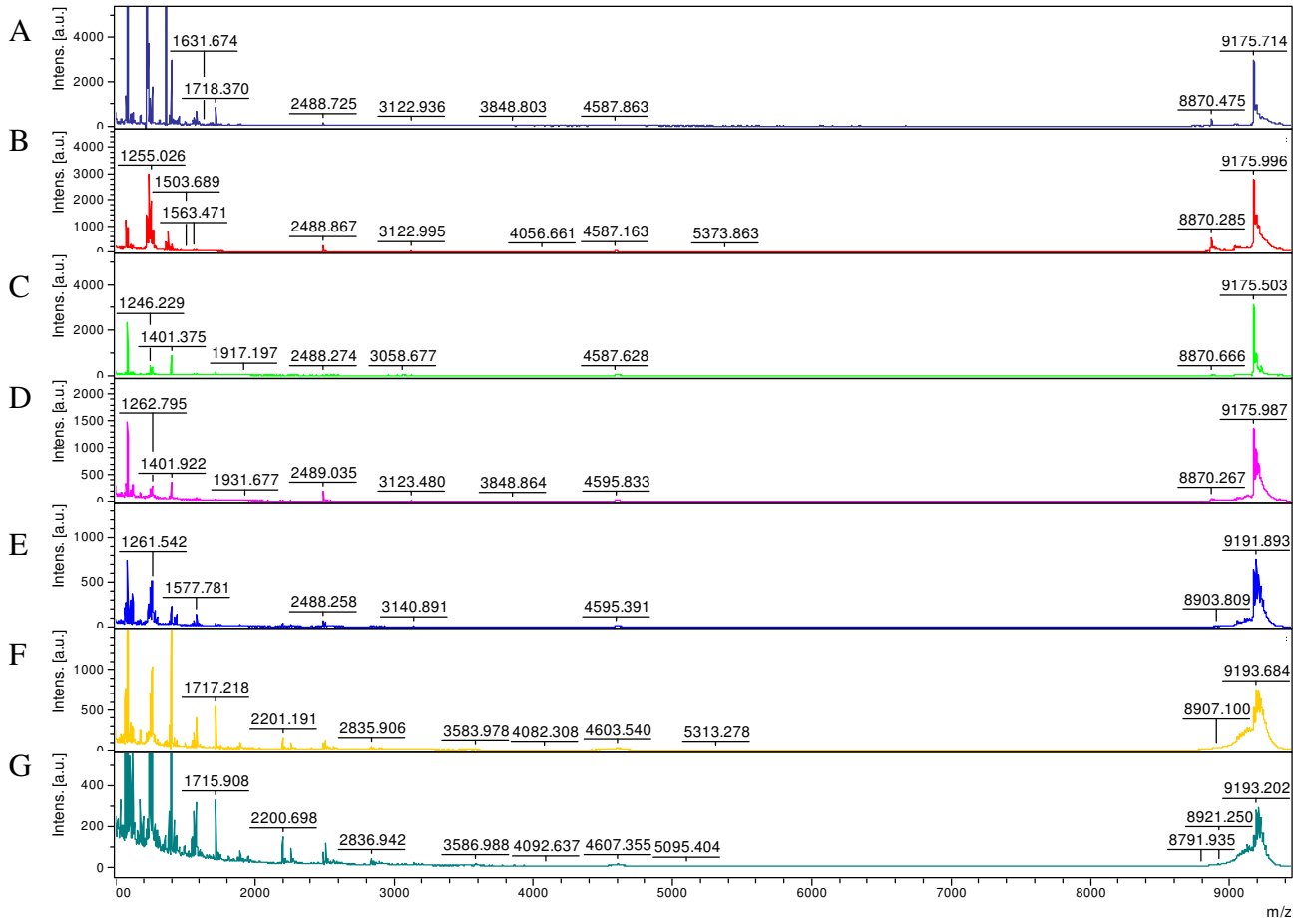

Figure SM21. MALDI-TOF mass spectra for time-dependent incubations of 10 µM Cu-PEP201, 1 mM H_2O_2/ascorbate, and 10 µM Fl-16S RNA at 37 ºC. (A) 0 min; (B) 10 min; (C) 20 min; (D) 30 min; (E) 60 min; (F) 90 min; (G) 120 min.

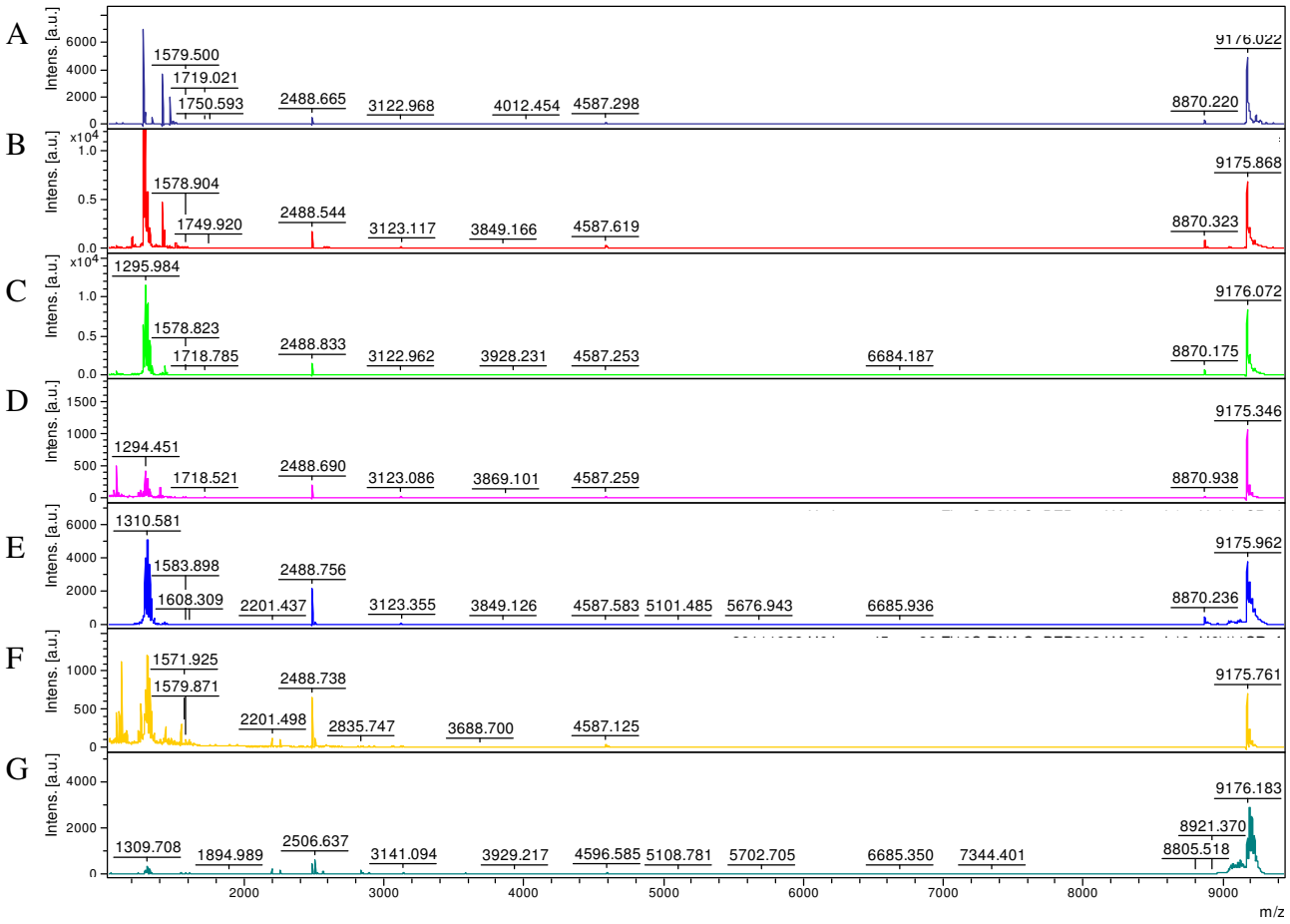

Figure SM22. MALDI-TOF mass spectra for time-dependent incubations of 10 µM Cu-PEP202, 1 mM H_2O_2/ascorbate, and 10 µM Fl-16S RNA at 37 ºC. (A) 0 min; (B) 10 min; (C) 20 min; (D) 30 min; (E) 40 min; (F) 60 min; (G) 90 min.

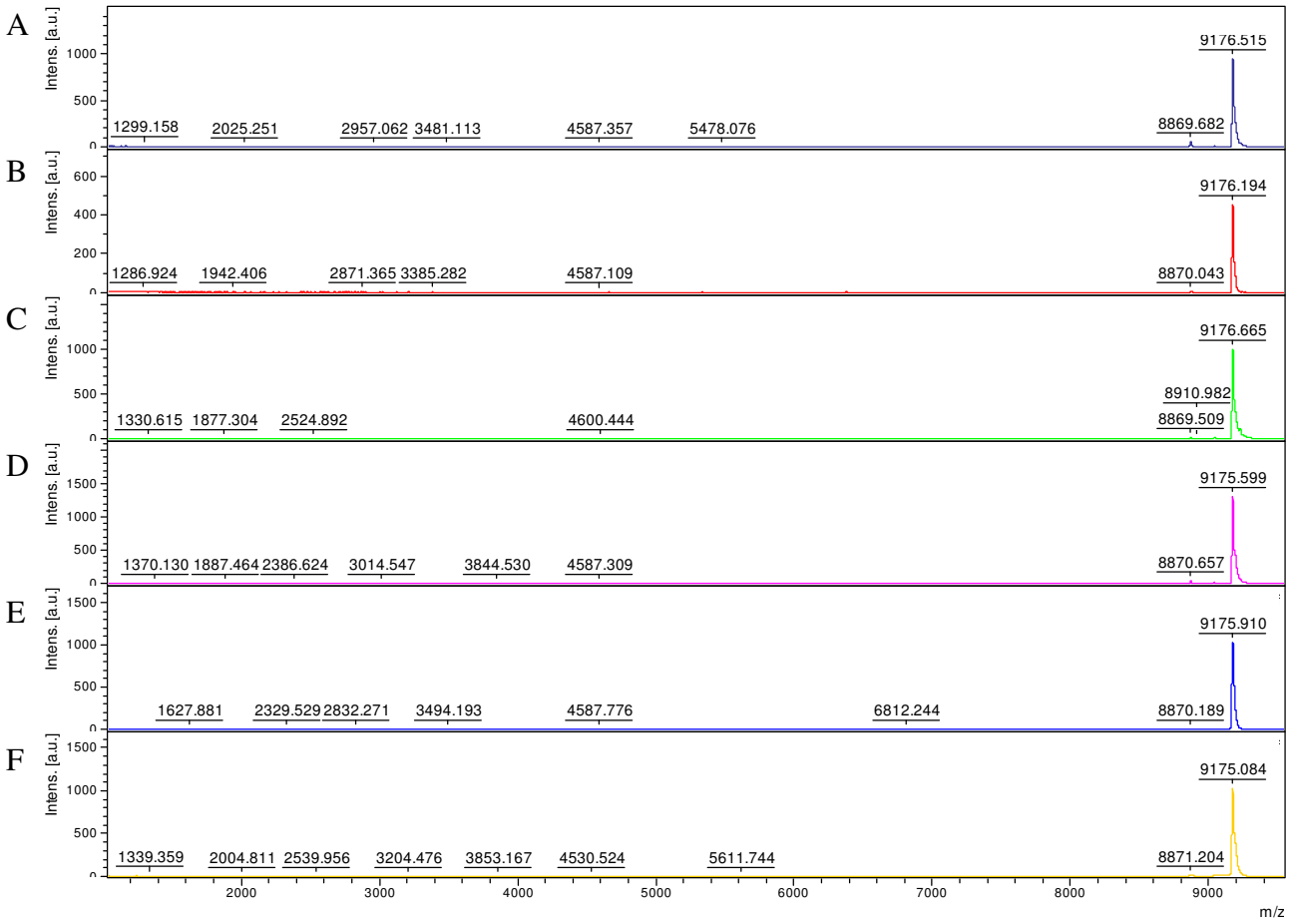

Figure SM23. MALDI-TOF mass spectra for time-dependent incubations of 10 µM Cu-PEP203, 1 mM H_2O_2/ascorbate, and 10 µM Fl-16S RNA at 37 ºC. (A) 0 min; (B) 10 min; (C) 20 min; (D) 30 min; (E) 60 min; (F) 120 min.

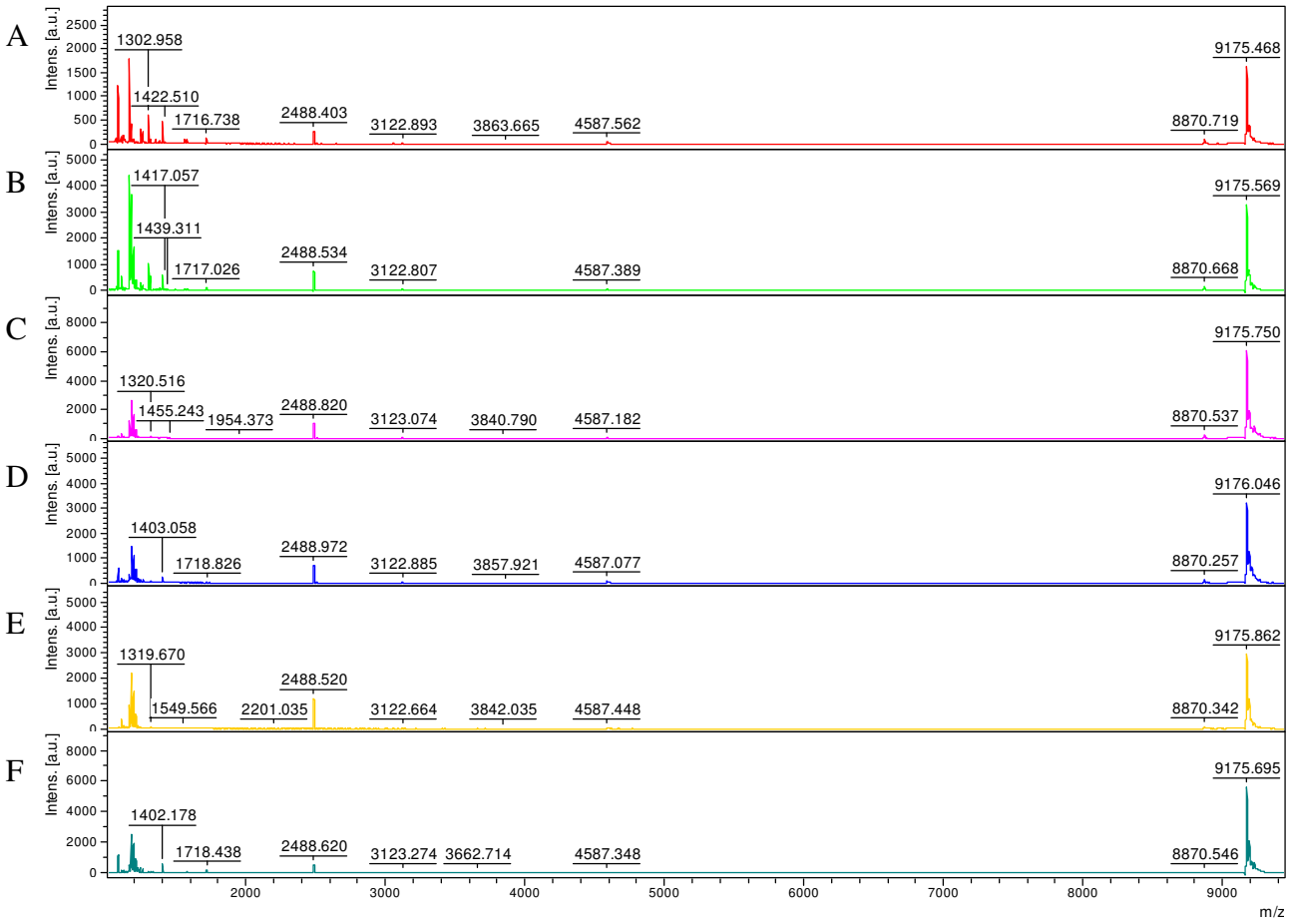

Figure SM24. MALDI-TOF mass spectra for time-dependent incubations of 10 µM Cu-PEP209, 1 mM H_2O_2/ascorbate, and 10 µM Fl-16S RNA at 37 ºC. (A) 10 min; (B) 20 min; (C) 30 min; (D) 60 min; (E) 90 min; (F) 120 min.

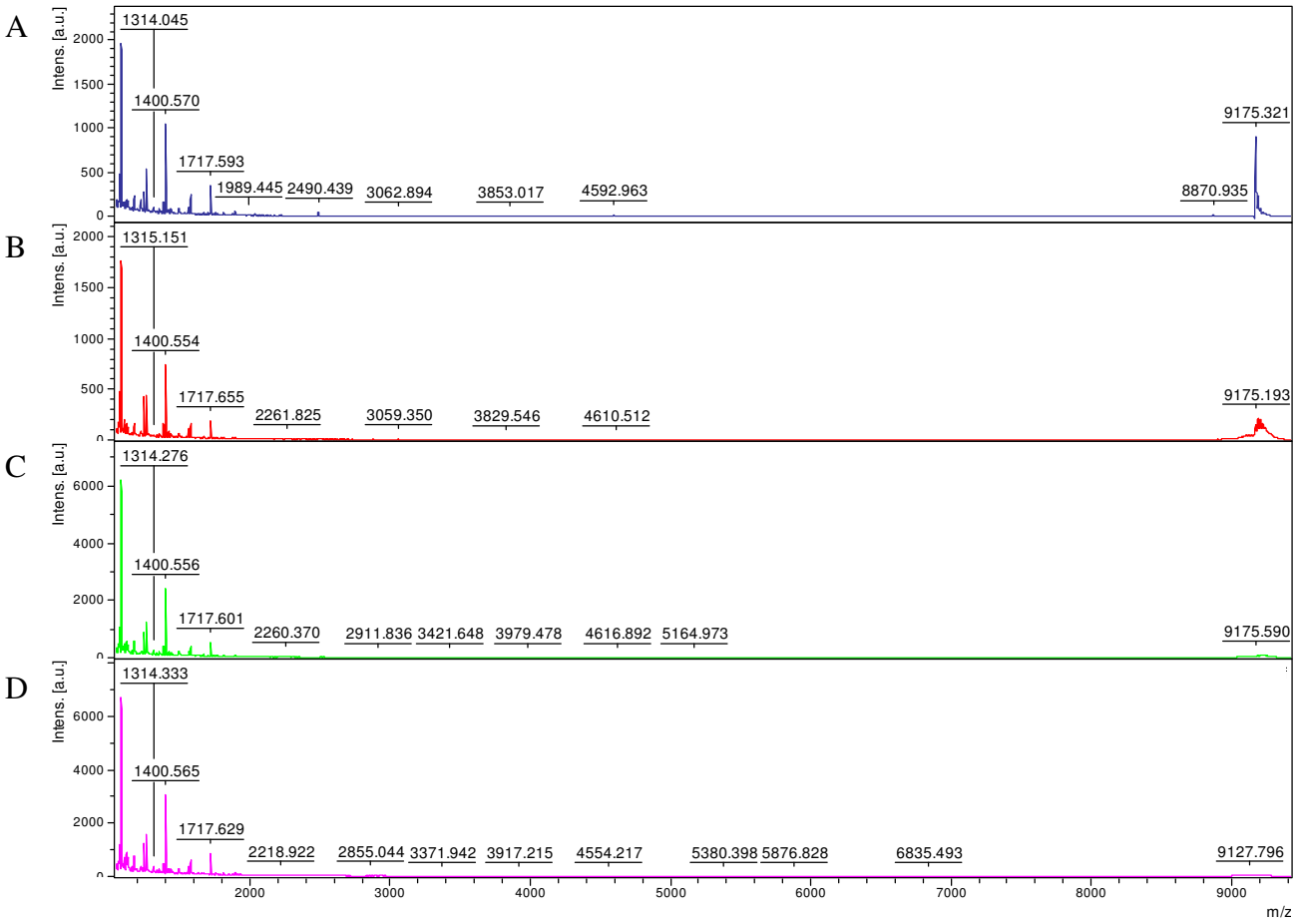

Figure SM25. MALDI-TOF mass spectra for time-dependent incubations of 10 µM free Cu, 1 mM H_2O_2/ascorbate, and 10 µM Fl-16S RNA at 37 ºC. (A) 0 min; (B) 5 min; (C) 10 min; (D) 20 min.

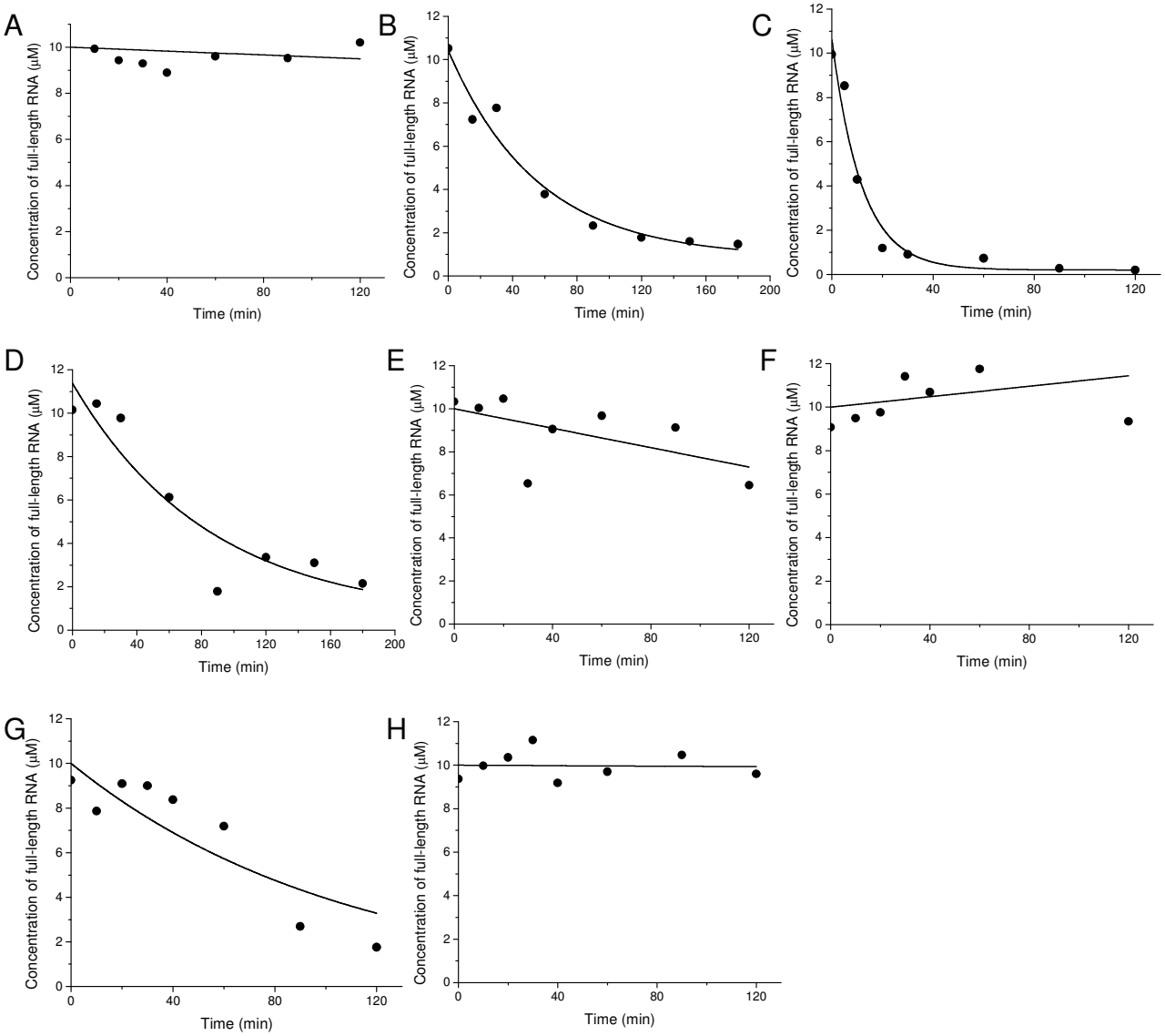

Figure SM26. PAGE analysis of time-dependent incubations of 10 μM Fl-16S RNA at 37 ºC with 1 mM H_2O_2/ascorbate and: (A) none; (B) 10 μM Cu-GGH; (C) 10 μM free Cu; (D) 10 μM Cu-PEP201; (E) Cu-PEP202; (F) Cu-PEP203; (G) Cu-PEP204; (H) Cu-PEP209. The disappearance of full-length Fl-16S RNA over time was fit to a first-order decay model in order to obtain initial rates of cleavage (nM/min).

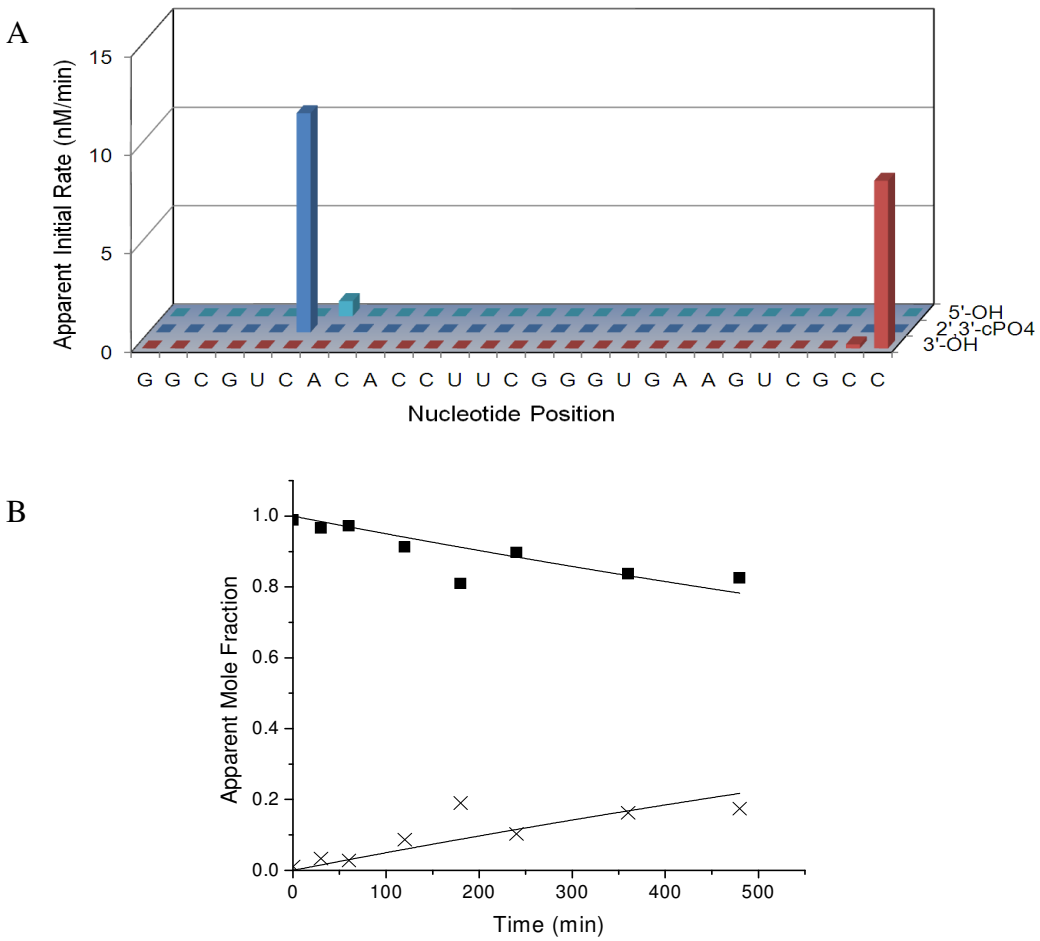

Species (direction)	Obsd. m/z (Da)	Initial rate from MALDI-TOF MS (nM/min)	Initial rate from PAGE (nM/min)
Fl-16S RNA (disappearance)	9175.7	9 ± 4	5 ± 1 (■)
5'-Fl-6mer (appearance)	2488.6	11 ± 4	5 ± 1 (×)
3'-21-mer (appearance)	6686	0.8 ± 0.2	Not labeled

Figure SM27. Comparison of (A) MALDI-TOF MS vs (B) PAGE analysis for the kinetics of cleavage of 10 µM Fl-16S RNA by 10 µM PEP204. Cleavage occurs at a single site, giving two RNA fragments of different mass. Disappearance of full-length RNA and the appearance of products were monitored by both MALDI-TOF MS and PAGE, and the initial rates were compared between the two assays, demonstrating the semi-quantitative ability of the MALDI-TOF MS method.

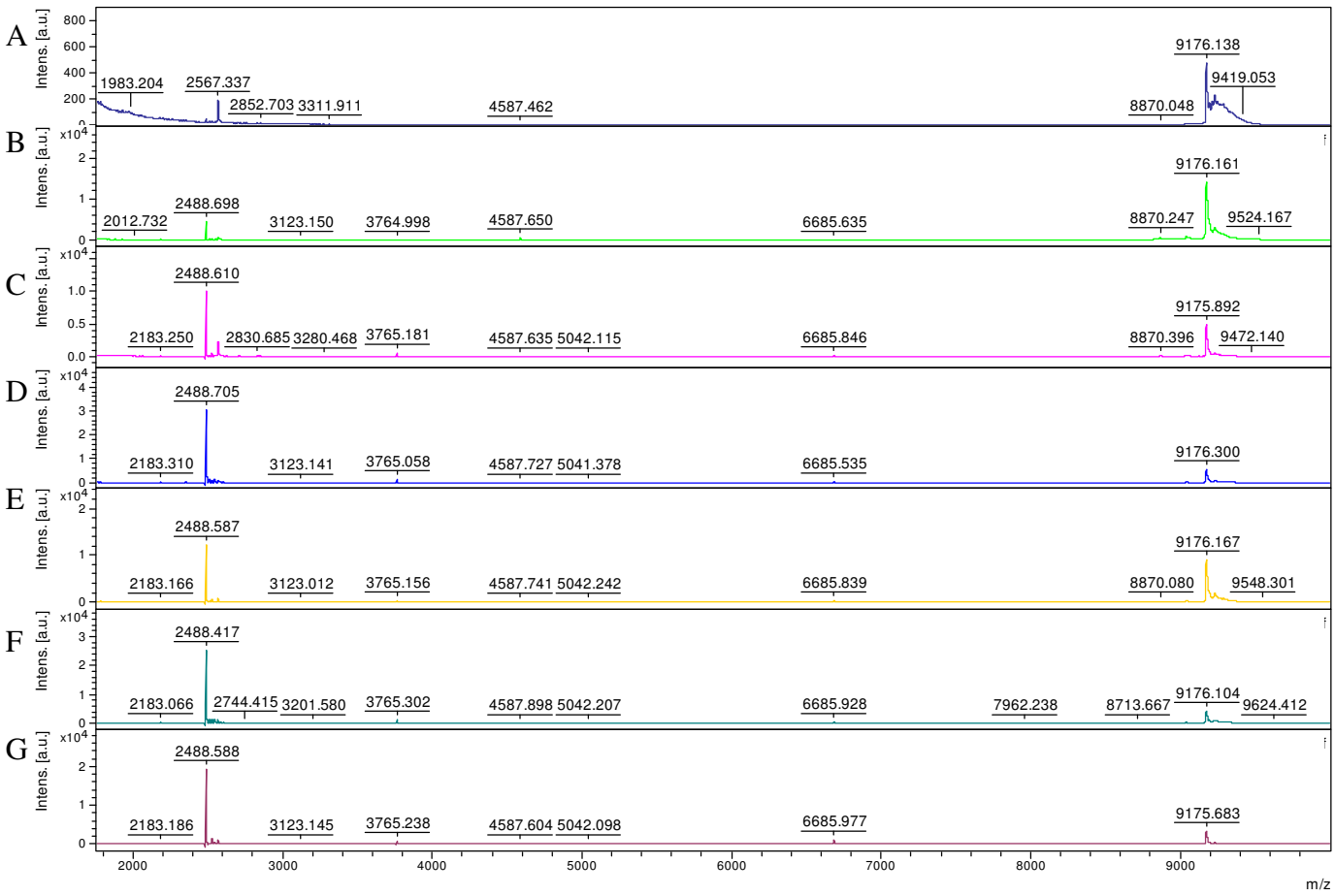

Figure SM28. MALDI-TOF mass spectra for time-dependent incubations of 10 µM PEP204 and 10 µM Fl-16S RNA at 37 ºC (the reaction shown in Figure SM27). (A) 0 min; (B) 60 min; (C) 120 min; (D) 180 min; (E) 240 min; (F) 360 min; (G) 480 min.

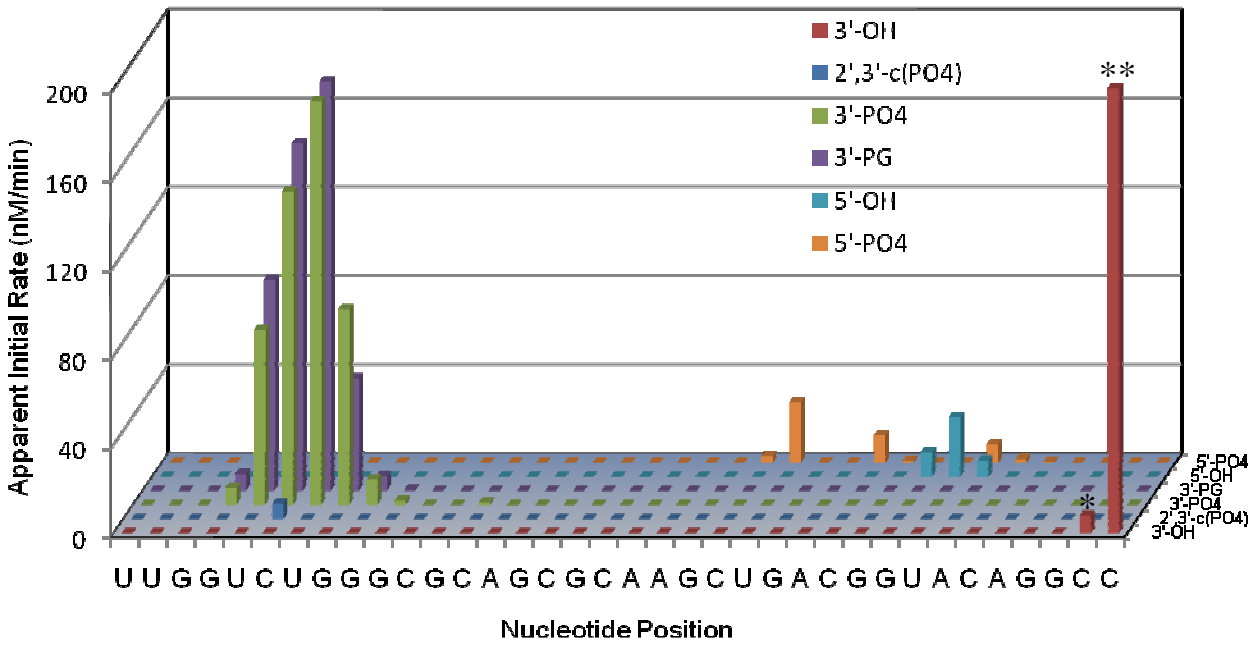

Figure SM29. Apparent initial rates of formation of RNA fragments containing the listed overhangs at the listed nascent termini, resulting from cleavage of 10 µM Fl-RRE RNA by 10 µM Fe-EDTA-Rev, 1 mM H_2O_2, and 1 mM ascorbate. Apparent initial rates of disappearance of the full-length 36-mer Fl-RRE RNA (**) and the 35-mer impurity (*) were 660 nM/min (abbreviated in figure) and 8 nM/min, respectively.

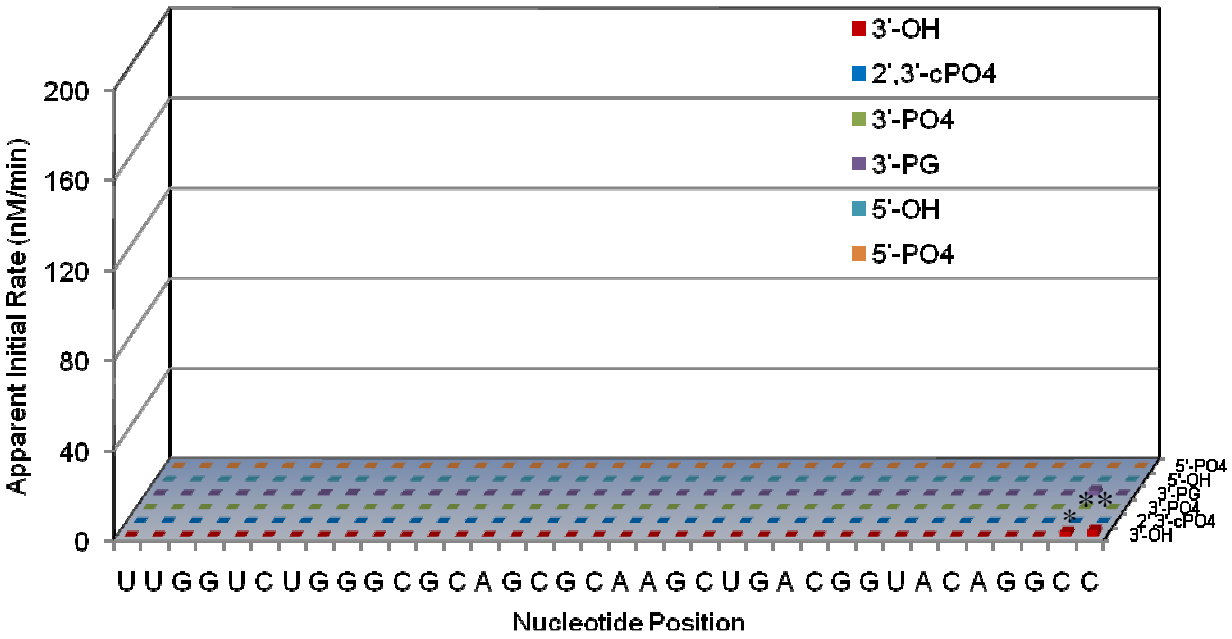

Figure SM30. Apparent initial rates of formation of RNA fragments containing the listed overhangs at the listed nascent termini, resulting from cleavage of 10 μM Fl-RRE RNA by 1 mM H_2O_2 and 1 mM ascorbate, but lacking added catalyst. Effectively no cleavage was observed in the absence of catalyst. Apparent initial rates of disappearance of the full-length 36-mer Fl-RRE RNA (**) and the 35-mer impurity (*) are also shown.

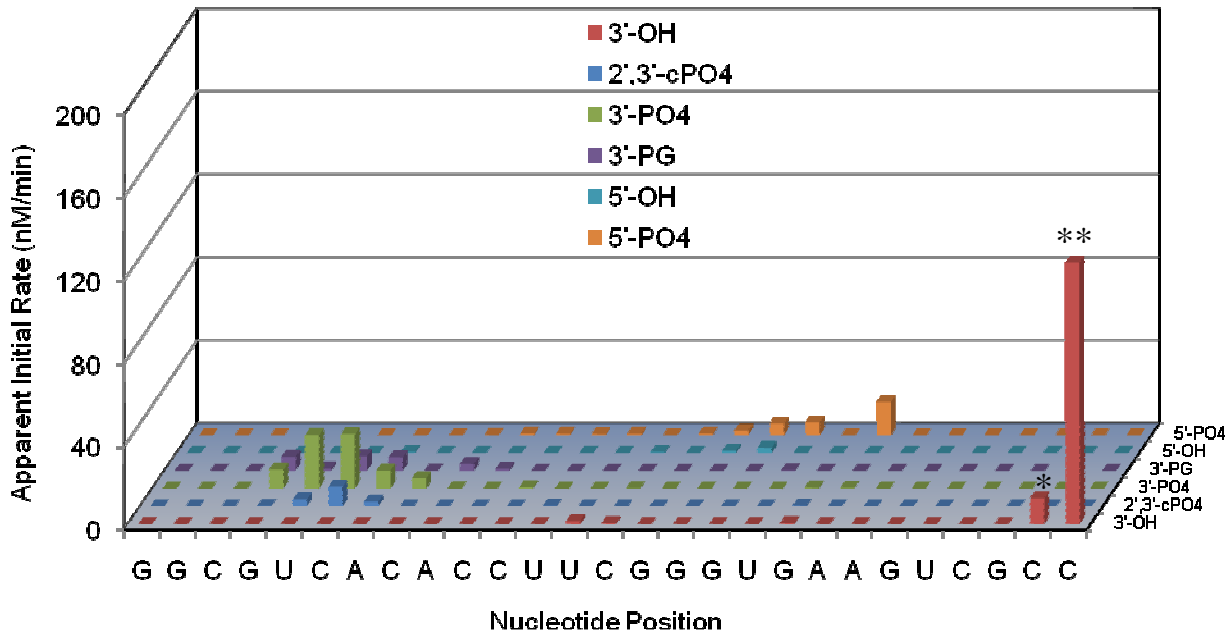

Figure SM31. Apparent initial rates of formation of RNA fragments containing the listed overhangs at the listed nascent termini, resulting from cleavage of 10 µM Fl-16S RNA by 10 µM Cu-GGH, 1 mM H_2O_2, and 1 mM ascorbate. Apparent initial rates of disappearance of the full-length 27-mer Fl-16S RNA (**) and the 26-mer impurity (*) are also shown.

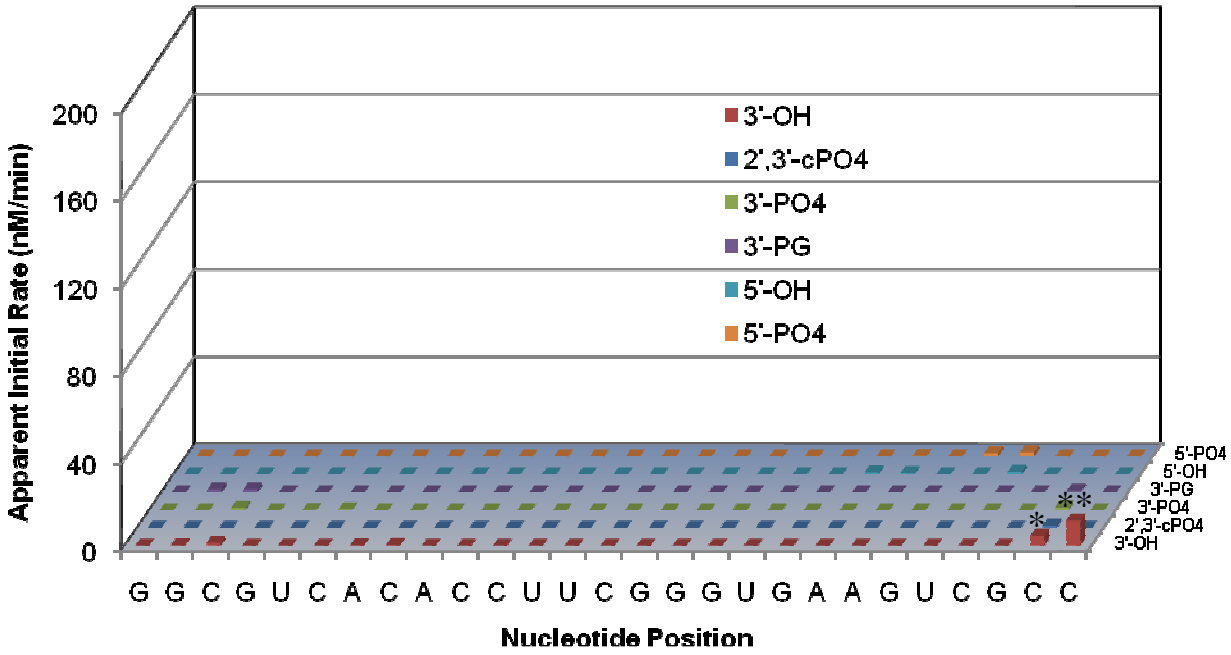

Figure SM32. Apparent initial rates of formation of RNA fragments containing the listed overhangs at the listed nascent termini, resulting from cleavage of 10 μM Fl-16S RNA by 1 mM H_2O_2 and 1 mM ascorbate, but lacking added catalyst. Effectively no cleavage was observed in the absence of catalyst. Apparent initial rates of disappearance of the full-length 27-mer Fl-16S RNA (**) and the 26-mer impurity (*) are also shown.

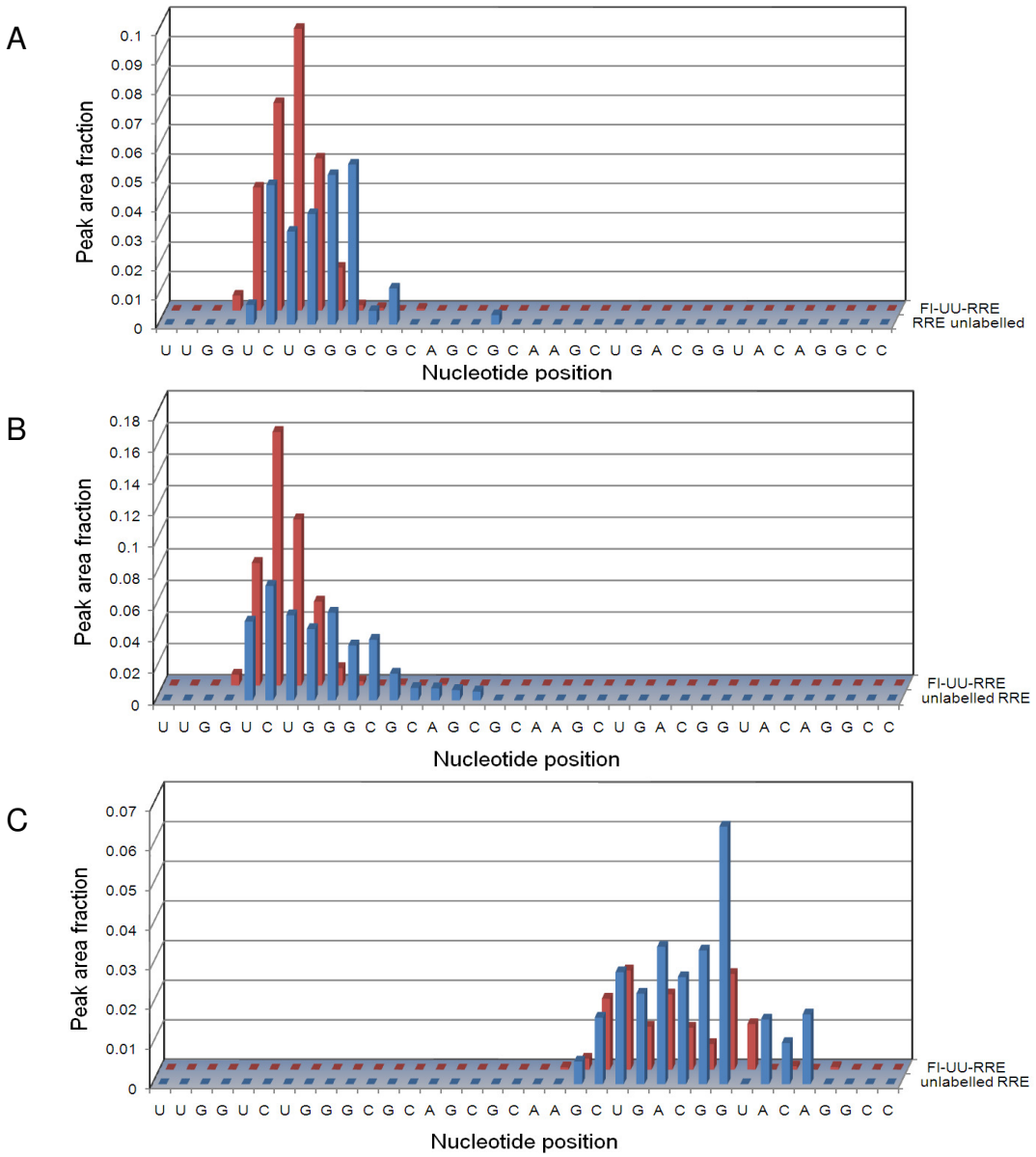

Figure SM33. Comparison of Fl-RRE RNA (red, 36-mer) vs unlabelled RRE RNA (blue, 34-mer lacking 5'-Fl-UU). Catalyst Fe-EDTA-Rev (10 μM) and H_2O_2/ascorbate (1 mM) were incubated for 1 h with 10 μM of either Fl-RRE RNA or unlabelled RRE RNA, and the peak area fractions of all products were determined. (A) RNA cleavage fragments containing nascent terminal 3'-phosphates; (B) cleavage fragments containing nascent terminal 3'-phosphoglycolates; (C) cleavage fragments containing nascent terminal 5'-phosphates.

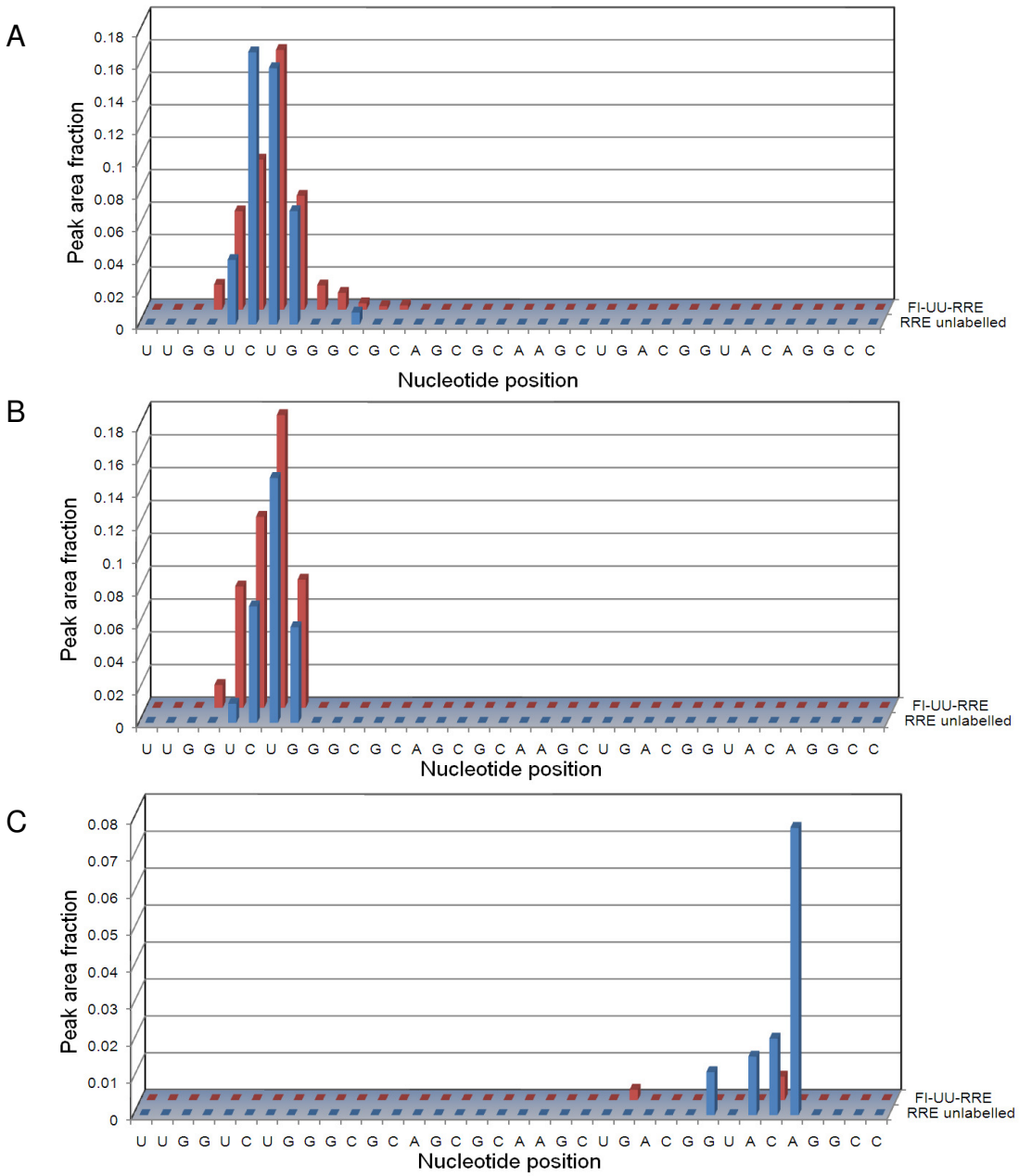

Figure SM34. Comparison of Fl-RRE RNA (red, 36-mer) vs unlabelled RRE RNA (blue, 34-mer lacking 5'-Fl-UU). Catalyst Cu-NTA-Rev (10 μM) and H_2O_2/ascorbate (1 mM) were incubated for 1 h with 10 μM of either Fl-RRE RNA or unlabelled RRE RNA, and the peak area fractions of all products were determined. (A) RNA cleavage fragments containing nascent terminal 3'-phosphates; (B) cleavage fragments containing nascent terminal 3'-phosphoglycolates; (C) cleavage fragments containing nascent terminal 5'-phosphates.

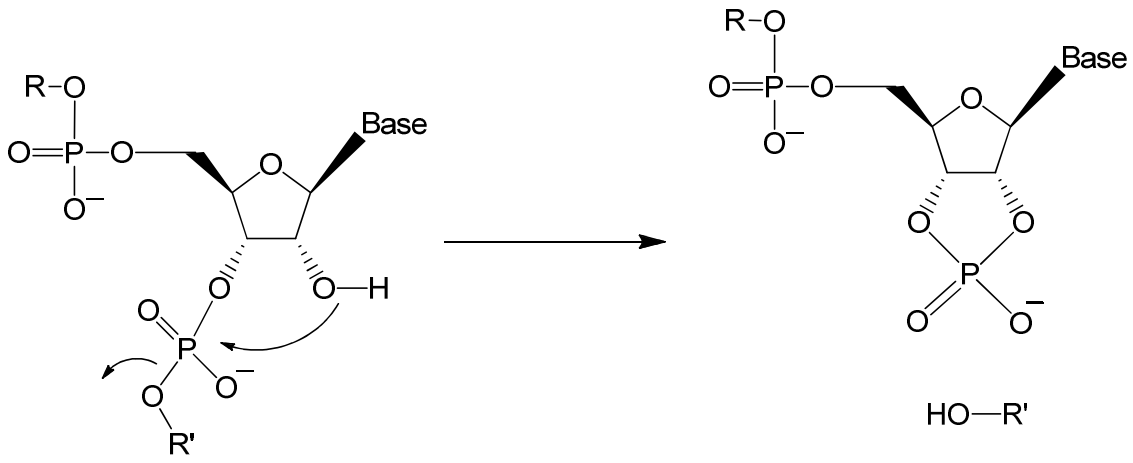

Figure SM35. Proposed mechanism for 2'-OH-mediated endonucleolytic cleavage of RNA to give fragments containing nascent 2',3'-cyclic phosphate or 5'-hydroxyl termini (c-fragments or y-fragments, respectively).

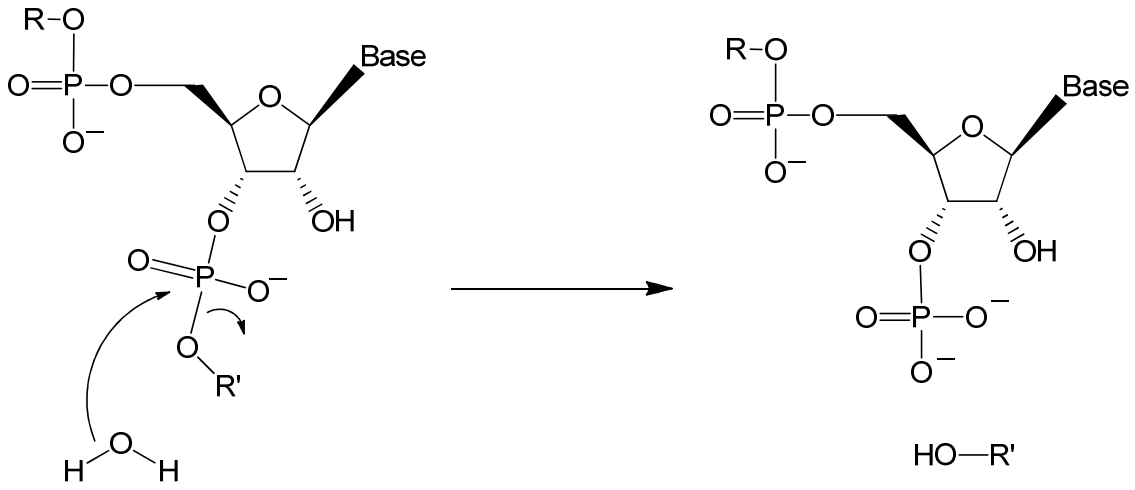

Figure SM36. Proposed mechanism for possible hydrolysis of RNA to give fragments containing nascent 3'-phosphate and 5'-hydroxyl termini (d-fragments and y-fragments, respectively). The mechanism may involve a 2',3'-cyclic phosphate intermediate, if the reaction occurs by 2'-OH-mediated attack; if this occurs, a 2'-phosphate is expected to result, in approximately equal abundance to the 3'-phosphate. It is also possible for hydrolysis to give fragments containing nascent 5'-phosphate and 3'-hydroxyl termini, depending on which P-O bond is hydrolyzed.

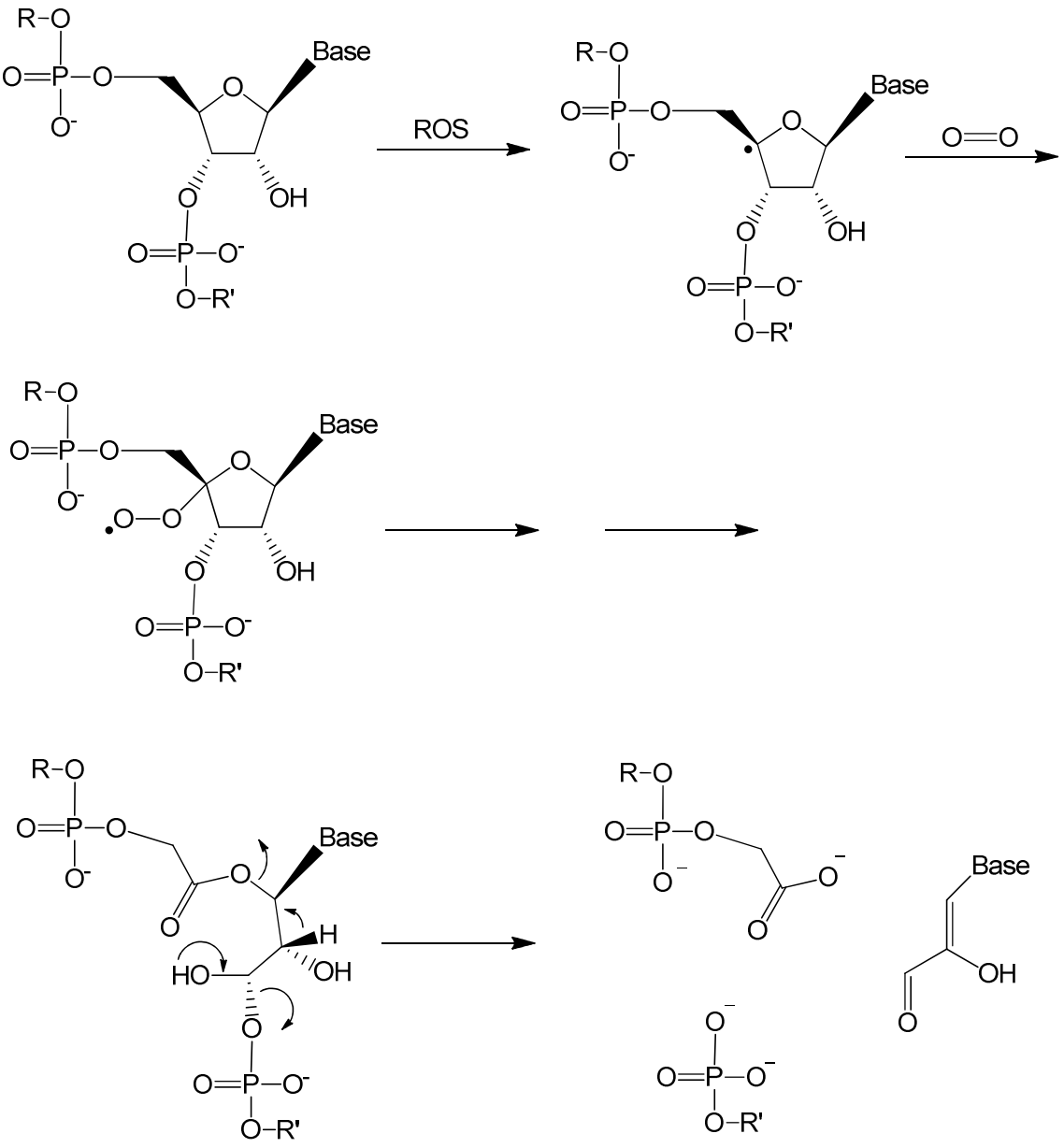

Figure SM37. Proposed mechanism for H-4 abstraction mediated by ROS generated by catalytic metal centers under aerobic conditions, observed by formation of 3'-phosphoglycolate and 5'-phosphate products. Slight mechanistic variations are possible that give the same RNA fragments.

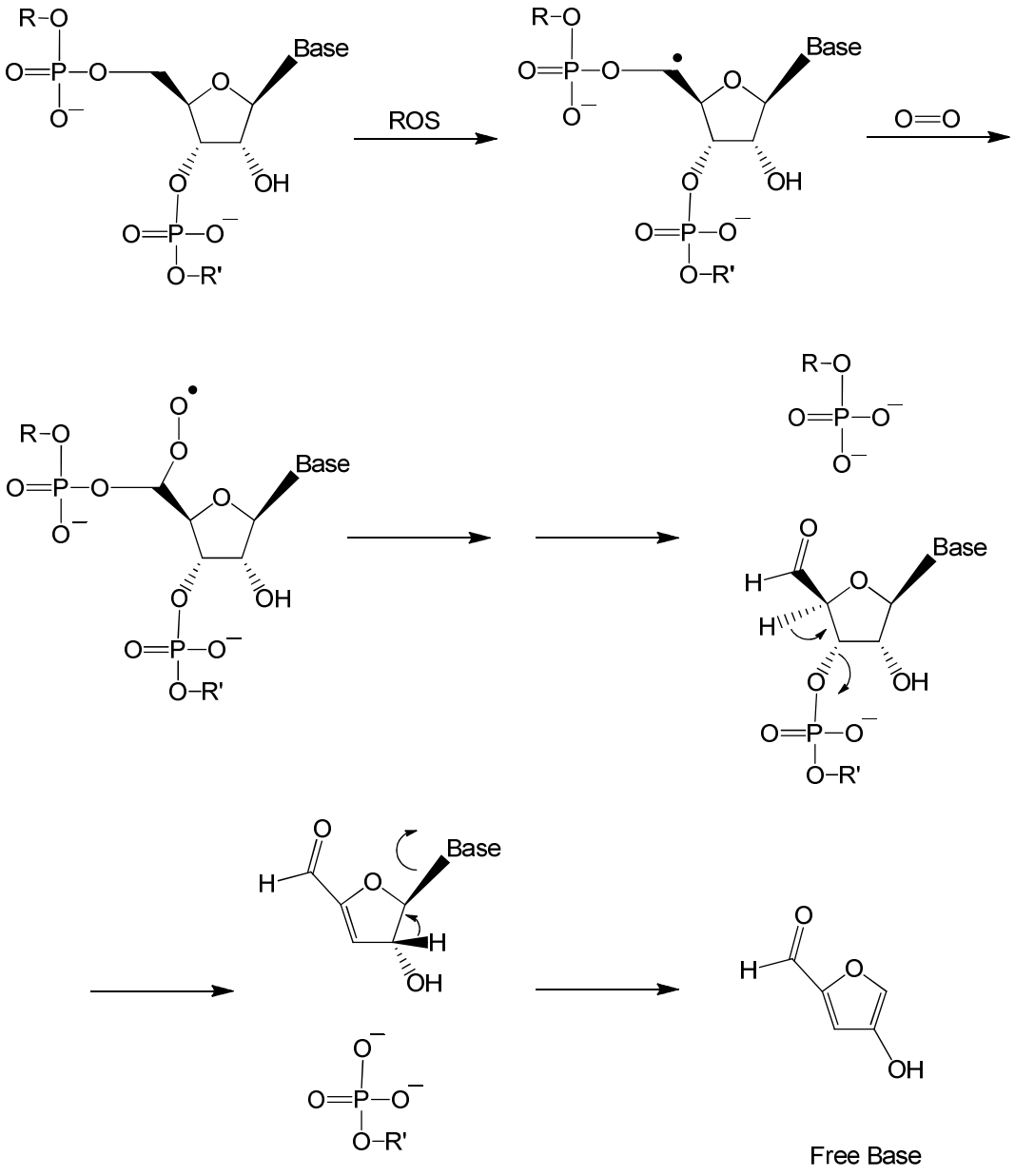

Figure SM38. Proposed mechanism for H-5 abstraction mediated by ROS generated by catalytic metal centers under aerobic conditions, observed by formation of 3'-phosphate products. The last two steps require additional heating. Slight mechanistic variations are possible that give the same RNA fragments.

```
#!/usr/bin/perl


print "\n";
print "\n";
print "Welcome to MassDaddy by Jeff Joyner, 2011\n";
print "\n";
print "Please enter the name of the file, with extension, containing the predicted masses.\n";

# enter file name
my $predmass = <>;

print "\n";
print "Please enter the name of the mass list file, with extension.\n";

# enter file name
my $masslist = <>;

# enter mass tolerance
print "\n";
print "Please enter the +/- mass tolerance for peak detection (ppm).\n";
my $tol = <>;

print "Please enter the desired filename of your output file.\n";

# enter file name
my $output = <>;


open output, ">$output";
print output "TheorMass\tObsdMass\tMassError(ppm)\tPosition\tOverhang\tPeakArea\n";



########## The first section organizes matched MS peaks by nucleotide position and overhang type
 open (predmass, "$predmass");
 my(@pred) = <predmass>; # read predicted mass file into list

   foreach $pred (@pred)
       {
        @predcolumns = split("\t", $pred);

       open (masslist, "$masslist");
       my(@list) = <masslist>; # read masslist into list

       foreach $list (@list) # loop thru list
               {
                @listcolumns = split("\t", $list);

               $high = $predcolumns[0] + ($predcolumns[0] * $tol / 1000000);
                $low = $predcolumns[0] - ($predcolumns[0] * $tol / 1000000);
               if ($listcolumns[0] < $high)
                                {
                                if ($listcolumns[0] > $low)
                                                {
                                                $error = ($listcolumns[0] - $predcolumns[0]) * 1000000 / $predcolumns[0];
                                                print output "$predcolumns[0]\t$listcolumns[0]\t$error\t$predcolumns[1]\t$predcolumns[2]\t$listcolumns[5]\n";
                                                $error = 999999999;
                                                }

                                }

               }
         close (masslist, "$masslist");
                if ($error != 999999999)
                                {
                                print output "$predcolumns[0]\tno match\tno match\t$predcolumns[1]\t$predcolumns[2]\t0\n";
                                $error = 111111111;
                                }
                $error = 22222222;
        }

 close (predmass, "$predmass");
```

```
############ The following section organizes unmatched MS peaks
open (masslist, "$masslist");
my(@list) = <masslist>; # read masslist into list


 foreach $list (@list) # loop thru list
		{
		@listcolumns = split("\t", $list);

		open (predmass, "$predmass");
		my(@pred) = <predmass>; # read predicted mass file into list

		foreach $pred (@pred)
			{
			@predcolumns = split("\t", $pred);
			$high = $predcolumns[0] + ($predcolumns[0] * $tol / 1000000);
			$low = $predcolumns[0] - ($predcolumns[0] * $tol / 1000000);
			if ($listcolumns[0] < $high)
				{
				if ($listcolumns[0] > $low)
					{
					$error = 999999999;
					}

				}

			}
		close (predmass, "$predmass");
		if ($error != 999999999)
			{
			print output "unknown\t$listcolumns[0]\tunknown\tunknown\tunknown\t$listcolumns[5]\n";
			$error = 111111111;
			}
			$error = 22222222;
		}

 close (masslist, "$masslist");

#
```

Figure SM39. MassDaddy: Perl script code used for rapid automated assignment of mass spectra. MassDaddy requires user input of (1) a tab-delimited text file mass list containing observed m/z values (column 0 of 0-5) and peak areas (column 5 of 0-5) from a mass spectrum, as exported from Bruker FlexAnalysis software and saved by Microsoft Excel, (2) a tab-delimited text file containing (on each row) the predicted mass, the nucleotide position of the nascent overhang, and the identity of the nascent overhang, respectively, for each possible cleavage product (one product per row), and (3) the mass tolerance (ppm) used for matching. MassDaddy creates an output file for each spectrum with six columns (left to right): the theoretical m/z (Da), the observed m/z (Da), the mass matching error (ppm), the nucleotide position of the nascent overhang, the nascent overhang type, and the peak area, arranged by overhang type and sequence. Unassigned peaks are also provided in the output file. MassDaddy requires that Perl is installed on the computer and is used from the command prompt. Mass list files and predicted mass files must be placed in the same folder as MassDaddy before use. To use MassDaddy, copy the above text into a text file, and save as a .pl file.

ultrafleXtreme Series MALDI TOF/TOF Mass Spectrometers (Bruker)

Resolution: > 40,000

autoflex III Series MALDI-TOF & TOF/TOF Systems (Bruker)

Resolution: > 20,000
Mass Range: 700 to 5000 Da

Axima Assurance MALDI Time of Flight Mass Spectrometer (Shimadzu)

Resolution: >5000 FWHM
Mass Range: 1 kDa to 500 kDa

Axima Confidence MALDI TOF Mass Spectrometer (Shimadzu)

Resolution: 5000 FWHM in linear mode; 15000 FWHM in reflectron mode
Mass Range: 1 kDa to 500 kDa

Axima Performance MALDI TOF TOF Mass Spectrometer (Shimadzu)

Resolution: >20,000 FWHM (reflectron mode)
Mass Range: 1 kDa to 500 kDa

Figure SM40. Comparison of common MALDI-TOF mass spectrometers. Resolutions and mass ranges listed were given by manufacturers/vendors.

SM References

(1) McKenzie, J. L.; Duyvestyn, J. M.; Smith, T. B., K.; Mackay, J.; Cursons, R.; Cook, G. M.; Arcus, V. L. *RNA* **2012**, *18*, 1267.

(2) Joyner, J. C.; Cowan, J. A. *J. Am. Chem. Soc.* **2011**, *133*, 9912.